ADVANCES IN GEOPHYSICS, VOLUME 21

CLIMATIC EFFECTS OF CIRRUS CLOUDS

KENNETH P. FREEMAN[1] AND KUO-NAN LIOU

Department of Meteorology
University of Utah
Salt Lake City, Utah

1. INTRODUCTION

The realization in recent years that human endeavors are particularly vulnerable to uncertainties in climate, and that human activity may be causing climatic change even now, lends a special urgency to the need for deeper understanding of the climate of the Earth and the problems of assessing and predicting climate change. The human suffering resulting from the extended drought in the Sahel bears agonizing witness to the disastrous potential of climatic variability. As it happens, the climate of the planet is now in a particularly benign stage. Paleoclimatological and historical records show that the climate has not always been so benevolent. The last ice age, of 20,000 years ago, when kilometer-thick glaciers covered parts of the northern hemisphere as far south as 40° latitude, and

[1] Present address: Air Force Global Weather Central, Offutt AFB, Nebraska 68113.

ISBN 0-12-018821-X

the "little ice age" of historical times demonstrate this reality in a manner most convincing.

The climate of the planet is a complex combination of time-mean states of a large array of parameters, both internal and external to the Earth–atmosphere system. Schneider and Dickinson (1974) have reduced to three the number of fundamental physical factors that determine the climate. These are the input of solar radiation, the composition of the atmosphere, and the Earth's surface characteristics. The primary effect of these factors is the role they play in determining the radiation balance of the atmosphere and the Earth. Over a sufficiently long time, the absorbed solar radiation must be balanced by the outgoing terrestrial radiation. On the global average and over a long time interval, this balance seems to be maintained, but on the smaller scale in time and space this is not generally true. The temporary imbalances in the radiative budget result in differential heating of the globe which, coupled with the rotation of the Earth, drives the circulation of the atmosphere and the ocean currents. These circulations in turn regulate the distributions of temperature, cloudiness, and precipitation over the globe. Understanding of climate and the mechanisms of climate change must begin with detailed understanding of the radiative balance of the atmosphere and Earth and of the factors which influence that balance sufficiently to cause long-term changes in the climate.

The most important regulators of the radiation balance are clouds, which regularly occupy at least 50% of the sky on a global scale. Clouds absorb and scatter the incoming solar radiation and emit thermal radiation according to their temperatures. The climatological horizontal extent of the cloud cover, the percent of the sky covered by clouds, has a very strong impact upon the radiation balance of the Earth–atmosphere system. Local variations in cloudiness are a natural, regularly occurring phenomenon, of only transient local importance to the radiation balance. Such local changes are due to the changing synoptic-scale conditions embedded in the general circulation. Long-term, secular changes in cloudiness are difficult to detect, especially since, until rather recently, observations have been almost exclusively ground-based and subject to the attendant errors.

Evidence of changes in global average cloudiness does not exist at present, but there may exist evidence that more localized cloudiness has increased. Machta and Carpenter (1971) reported on secular increases in the amount of high cloud cover in the absence of low or middle clouds. The authors reported increases in the cirrus cloudiness at a number of stations in the United States between 1948 and 1970. It has been suggested (Study of Man's Impact on Climate, 1971) that there may be a link between this increase in cloudiness and the expansion of jet aircraft

flights in the upper troposphere and lower stratosphere. If this link does exist, then the projected increase of jet aircraft traffic in the next two decades may cause a large increase in cirrus cloudiness, particularly over North America, the north Atlantic, and Europe, in the latitude range between 30° and 65° north.

Such an increase in cloudiness may have serious implications for the radiation balance of the Earth's atmosphere and consequent impact upon the planetary climate. A significant increase in cirrus clouds should serve to raise the Earth's albedo over the affected regions and thereby reduce the absorption of solar radiation. More serious results might follow should the radiation balance be upset sufficiently to allow some feedback process to amplify the effects. Schneider and Dickinson (1971) identify at least seven feedback or coupled mechanisms operating in the climatic balance.

The purpose of this article, then, is to report on an investigation of the radiative balance of the Earth-atmosphere systems, its sensitivity to cloud and aerosol scattering, and the impact which an increase in cirrus cloudiness might have upon that balance. The research program was carried out by constructing a model of the Earth's atmospheric radiation budget and then varying the cirrus cloud cover in accordance with hypothetical projections. The accuracy of the radiation budget was determined by comparisons with earlier calculations and with satellite observations of the radiation balance parameters. The radiation budgets of the northern and southern hemispheres are investigated simultaneously utilizing an accurate radiative transfer technique. The changes in heating and cooling rates, zonally averaged albedo, atmospheric absorption, emission and transmission of the radiation, and the radiative budgets for the top, bottom, and within the atmosphere were then calculated and analyzed.

The next section presents a critical analysis of previous atmospheric radiation and heat budget studies, including the comprehensive studies by London (1957), and Katayama (1967a,b) of the northern hemisphere, and Sasamori *et al.* (1972) of the southern hemisphere. The third section is a discussion of the radiative and pertinent physical properties of the global atmosphere and the solution of the radiative transfer equation employed in this work. Section 4 is a discussion and analysis of the global heat and radiation budgets and comparisons with earlier calculations and satellite observations. Finally, the fifth section will present results obtained by including increasing amounts of cirrus cloudiness in the model.

2. Review of Previous Work

Present knowledge about the radiation balance of the Earth dates largely from the work of Simpson (1928) and Baur and Phillips (1934).

These earliest results were based on a great many simplifying assumptions and very sketchy data, especially concerning the emission and absorption of terrestrial longwave radiation (Houghton, 1954). The work of these earlier researchers on atmospheric absorption of solar radiation was based largely on work done by the Smithsonian Institution. Simpson, for example, used a value of the planetary albedo of 0.43, taken from results of work at the Smithsonian.

Simpson recognized the importance of the spectral distribution of water vapor absorption and used a simple model of the atmosphere, based on rather crude data, to calculate the latitudinal and seasonal distributions of the radiative balance. However, he chose to consider only water vapor absorption of longwave radiation, thus ignoring the important contributions made by CO_2 and O_3 in the upper atmosphere. Furthermore, since he lacked sufficient information about the absorption properties of water vapor, he attempted to deduce them from attempts to balance the computed upwelling planetary radiation flux with the incoming solar radiation, wherein he used a value for the Earth's albedo of 0.43 and assumed no distribution of albedo with latitude. As a result, Simpson obtained a very flat latitudinal distribution of outgoing infrared flux at the top of the atmosphere.

Baur and Phillips improved upon Simpson's work by integrating the equations of radiative transfer to obtain a more realistic physical model. Their independent calculations of the global albedo led to a description of the variation of the albedo with latitude, but their mean global albedo was computed to be the same value as that used by Simpson.

With more detailed and extensive information about the absorption spectrum of water vapor and infrared transmission provided by the work of Elsasser (1938) and Schnaidt (1939), improved versions of atmospheric radiation charts were produced by Elsasser (1942) and Möller (1943). Elsasser's chart, however, did not properly account for the pressure dependency of absorption. Yamamoto (1950), using later calculations of the water vapor absorption spectrum produced an additional radiation chart.

Houghton (1954) made comprehensive calculations of the annual heat balance of the northern hemisphere, relying upon the Elsasser chart to compute the upwelling flux at the top of the atmosphere and upon observations from a pyrheliometric network to derive the solar radiation reaching the surface. Absorption by ozone was neglected, but Rayleigh scattering and absorption and scattering by aerosols were also considered, although somewhat crudely parameterized. He did perform a useful computation of zonally averaged surface albedos, which had not been done at that time, and using the available information about cloud albe-

dos, computed reasonable values for the mean annual albedo of the hemisphere and zonally averaged latitude belts. His planetary albedo was determined to be 0.34. The primary shortcomings of his work were the lack of calculations of absorption and emission in the upper atmosphere by ozone and carbon dioxide, the lack of accurate computations for aerosol and cloud scattering, and the cloud albedos used, which are at variance with more recent values.

London (1957) developed a radiation balance model for the northern hemisphere which included results for the vertical, latitudinal, and seasonal distributions of radiative heating and cooling and vertical fluxes of solar and planetary radiation. The Elsasser diagram was again used to calculate longwave upward flux, while empirical expressions for the absorption and scattering of solar radiation were employed. Scattering by clouds was ignored, and Rayleigh and aerosol scattering treated in a simple manner. Ozone and CO_2 effects were not considered. London used a cloud distribution consisting of heights and thicknesses of six cloud types, along with their climatological values of fractional cloudiness at 10° latitude belts (Telegadas and London, 1954). This cloud climatology is the only one of its kind yet in existence, and was used in the present study. London calculated the total planetary albedo to be 0.35. The atmospheric heat budget presented by Davis (1963) included computations of net latent heat and sensible heat flux from the Earth's surface to the atmosphere for the latitude belt 20°N to 70°N. Infrared cooling was computed with the use of a number of approximations for intensity and flux transmittances. Solar heating rates were computed with the use of empirical expressions for absorption by water vapor, carbon dioxide, and ozone. Scattering by clouds and aerosols was not considered.

The radiation budget model of Katayama (1966, 1967a,b) for the northern hemisphere troposphere is extremely detailed and complete, including seasonal, latitudinal, zonal, and hemispheric distributions of the radiation and heating and a comprehensive discussion of energy balances. The tropospheric model did not consider ozone or carbon dioxide absorption, and graphical methods and the chart of Yamamoto were used to compute planetary radiation fluxes. In the longwave spectrum, clouds were treated as blackbodies, with the exception of cirrus, which was considered to be gray. In the solar spectrum, Katayama relied upon empirical equations integrated over the whole solar spectral range for absorption by water vapor, Rayleigh scattering, reflection by clouds, and depletion by dust. The effects of cloud scattering and aerosol scattering were accounted for only by simplified approximations. Katayama obtained a planetary albedo of 0.374, from which he subtracted 2.8% of the incident solar flux to account for absorption by stratospheric ozone, to obtain a corrected

value of 0.346, which is very close to the values of 0.34 and 0.35 obtained by Houghton and London, respectively. Katayama derived useful values for the latitudinal distribution of zonally averaged albedos for January and July in the northern hemisphere, which were used in the present study.

Rodgers (1967) calculated the radiative energy budget for the region 0°–70° north and from 1000 to 10 mb for January, April, July, and October. In this work, parameterized equations were used in both the solar and infrared spectra. For the thermal spectrum, Rodgers used a Goody random model, with the Curtis–Godson approximation for water vapor absorption. All clouds were assumed black for terrestrial radiation except cirrus, which he took to be 50% black. In the solar spectrum, Rodgers used a computer modeled ray-tracing technique, following individual rays through the atmosphere from the top to the final destination in the atmosphere, the surface, or back to space. The heating rates computed in Rodger's model roughly approximate the zonal cross sections obtained in the present work. Again, the shortcoming in Rodger's work is the lack of adequate means of handling the scattering by aerosols and clouds. For clouds, Rodgers used a single absorption coefficient throughout the entire solar spectrum.

The southern hemisphere had been largely ignored until Sasamori *et al.* (1972) performed their comprehensive radiation budget calculations. This study followed the general techniques of Houghton, London, and Katayama. Calculation of radiation fluxes in the vertical was reduced to integration of formulas for upward flux at the top of the atmosphere and downward flux at the bottom, therefore the study does not present vertical distributions of the radiative parameters. The cloud distributions used were taken from the work of van Loon (1972) for fractional cloud amount, and from Telegadas and London (1954) for heights of cloud top and base, since there is little data available for the southern hemisphere. These data were also used in the present work. Sasamori *et al.* do compare their results with computations of other researchers and with the satellite observations of Vonder Haar and Suomi (1971). The results of the present work are, in turn, compared with the calculations of Sasamori *et al.* and with the satellite observations. The planetary albedo computed for the southern hemisphere by Sasamori *et al.* is 0.347.

Dopplick (1972) reported a study of radiative heating of the global atmosphere, in which were provided monthly and annual zonal mean global heating rates in the form of latitudinal cross sections. Dopplick also presented seasonal profiles of the contribution of each atmospheric constituent. For his calculations in the infrared, Dopplick used a Goody random model fitted in 20 spectral intervals and combined that with a continuum absorption and the Curtis–Godson approximation to represent

water vapor transmission. Empirical fits to measured absorption bands were used to model solar radiative transfer. Three classes of clouds, determined largely from satellite observations, were considered. Cloud scattering and scattering and absorption by aerosols were not considered at all.

A paper by Hunt (1977) addressed the sensitivity of the various components of the radiation balance to changes in cloud properties. Using a zonally averaged model atmosphere for both the northern and southern hemispheres, and a simple radiative transfer model of the sort to be used in a general circulation model, Hunt computed the sensitivity of solar heating and thermal cooling for various cloud conditions and various cloud radiative properties. This is a useful study in demonstrating the effects of various cloud parameterizations. However, the lack of information about the vertical structure of global cloud fields hampers his attempts to model the zonally averaged distribution of atmospheric heating. This same lack has characterized all attempts to model the global heat budget in detail, including the present work. Hunt does conclude that the atmospheric heating is highly sensitive to even small changes in cloud structure, a conclusion which is supported by the present study.

Satellite observations of the global radiation budget were reported by Vonder Haar (1968) and Vonder Haar and Suomi (1971) and were used in the present work as standards for comparison. Three very important radiation components were reported in these studies. These included the reflected solar flux, absorbed solar flux, and the upwelling longwave flux at the top of the atmosphere. Seasonal and annual latitudinal variations as well as global horizontal distributions of these components are presented, and provide convenient standards by which the success of the present radiation budget calculations can be judged. In addition to the two studies listed, the work of Raschke and Bandeen (1970) for June and July of 1966 was also used for purposes of comparison.

The primary shortcomings of the radiation budget models described above, in addition to the scarcity of data, a problem shared by all atmospheric radiation researchers, are in their handling of clouds and aerosols. Due to the nature of the methods used, scattering has been largely ignored and aerosols sometimes neglected entirely. One purpose of the present work has been to provide a method for considering both scattering and absorption properties of clouds and aerosols, and to demonstrate the effects that these factors may have on the radiation budget.

3. Radiative Transfer in the Atmosphere

In order to model the atmospheric radiation balance, the transfer of radiant energy through the atmospheric medium as described quantita-

tively by the radiative transfer equation must be computed. Many methods exist to perform these calculations, but few of these techniques meet the criteria of accuracy and efficiency, required in any scheme to be used in the extensive calculations involved in a radiation budget model. In the case of the solar radiation entering the atmosphere and being absorbed and scattered by the gas molecules, clouds, and aerosols, a detailed accounting must be kept for every spectral band and every layer in the model atmosphere. For thermal infrared radiation, the problem is somewhat simplified in that only flux calculations need to be performed in the clear atmosphere, since scattering computations are required only in very thin clouds such as cirrus.

To be useful for the purposes of the present study, a method of carrying out radiative transfer calculations must be relatively inexpensive in terms of computation time, since a great many calculations must be performed. For meteorological applications involving radiative transfer through clouds and aerosols in the atmosphere, the discrete ordinate method for radiative transfer, originally introduced by Chandrasekhar (1950) and further developed by Liou (1973a, 1974a) has been found quite efficient. The method allows for the solutions of the fundamental monochromatic radiative transfer equation to be derived explicitly and simplified. Further, the discrete ordinate method can easily take into account the distribution, thickness, and type of clouds and aerosols, making the scheme well suited to a study of the Earth's radiation budget.

3.1. *Method of Radiative Transfer*

The appropriate transfer equations describing the radiation field for the azimuthal independent diffuse intensity I may be written

$$\mu \frac{dI(\tau, \mu)}{d\tau} = I(\tau, \mu) - \frac{\tilde{\omega}_0}{2} \int_{-1}^{+1} P(\mu, \mu') I(\tau, \mu')\, d\mu' - \begin{cases} \dfrac{\tilde{\omega}_0}{4} F_0 P(\mu, \mu_0) \exp\left(\dfrac{-\tau}{\mu_0}\right) & - \text{SOL} \\ (1 - \tilde{\omega}_0) B_\nu(T) & - \text{IR} \end{cases} \tag{1}$$

where τ represents the optical depth, μ and μ_0 the cosine of the emergent and solar zenith angles, respectively, $\tilde{\omega}_0$ the single scattering albedo, F_0 the incident solar flux, T the temperature, P the normalized phase function, and B_ν the Planck function. Except T, μ, and μ_0, all parameters are wavelength or wave number dependent.

Employing the discrete-ordinates method for radiative transfer, the solutions of the transfer equations as shown by Liou (1973a) are given by

$$(2) \quad I(\tau, \mu_i) = \sum_j L_j \phi_j(\mu_i) \exp(-k_j \tau) + \begin{cases} Z(\mu_i) \exp(-\tau/\mu_0) & - \text{SOL} \\ B_\nu(T) & - \text{IR} \end{cases}$$

where i and j $(-n, n)$ denote the discrete streams (positive upward and negative downward) used in approximating the basic transfer equation, ϕ_j and k_j represent the eigenfunction and eigenvalue, respectively, the Z function is associated with Chandrasekhar's H function, the single scattering albedo and the expanded phase function in forms of Lengendre polynomials, and L_j's are coefficients to be determined from the boundary conditions.

The solutions of the radiative transfer equations given by Eq. (2) are applicable to a homogeneous and isothermal layer. Thus, in order to apply such solutions to inhomogeneous atmospheres, we divide the atmosphere into a number of sublayers each of which may be considered to be homogeneous and isothermal (Liou, 1975). At the top of the atmosphere, there is no downward diffuse intensity so that

$$(3) \quad I^1(0, -\mu_i) = 0$$

Between the layers, the intensities from all directions must be continuous. Thus,

$$(4) \quad I^l(\tau^l, \mu_i) = I^{l+1}(\tau^l, \mu_i), \qquad l = 1, 2, \ldots, N-1$$

where N is the total number of sublayers and τ^l represents the optical depth from the top of the atmosphere to the layer l. At the bottom of the atmosphere, the upward intensity is given by

$$(5) \quad I^N(\tau^N, +\mu_i) = \begin{cases} \dfrac{A_s}{\pi}\left[2\pi \sum_{i=1}^{n} a_i \mu_i I(\tau_N, -\mu_i) \right. \\ \left. + \pi \mu_0 F_0 \exp\left(\dfrac{-\tau_N}{\mu_0}\right)\right] & - \text{SOL} \\ B_\nu(T_s) & - \text{IR} \end{cases}$$

where A_s represents the surface albedo and T_s the surface temperature.

Upon inserting the intensity solution into Eqs. (3)–(5), a set of linear equations is obtained from which the unknown coefficients L_j for each sublayer may be determined by means of a matrix inversion technique. Once the constants of proportionality have been derived, then the intensity distribution at any level in the atmosphere may be evaluated. The next step is then to compute the upward and downward fluxes for each

layer. They are given by

$$F^{\uparrow}(\tau) = 2\pi \sum_{i=1}^{n} a_i \mu_i I(\tau, \mu_i)$$

$$F^{\downarrow}(\tau) = -2\pi \sum_{i=1}^{n} a_i \mu_i I(\tau, -\mu_i) - S(\tau, -\mu_0) \tag{6}$$

where

$$S(\tau, -\mu_0) = \begin{cases} \pi \mu_0 F_0 \exp(-\tau/\mu_0) & - \text{SOL} \\ 0 & - \text{IR} \end{cases} \tag{7}$$

The net flux for a given layer may be computed from

$$F_N(\tau) = F^{\uparrow}(\tau) + F^{\downarrow}(\tau) \tag{8}$$

and the heating or cooling rate for a layer of air resulting from the absorption by atmospheric gases and cloud and aerosol particles can be calculated from

$$\left(\frac{\partial T}{\partial t}\right)^{l} = -\frac{1}{\rho C_p}\left(\frac{\partial F_N}{\partial Z}\right)^{l} = \frac{\sigma_e}{C_p}\frac{F_N(\tau) - F_N(\tau + \Delta\tau)}{\Delta\tau} \tag{9}$$

where $\Delta\tau = \rho\sigma_e \Delta Z$, σ_e represents the extinction coefficient, ρ the air density, and C_p is the specific heat of air for constant pressure. Computations of the reflection, absorption, and transmission of solar radiation and heating and/or cooling rates covering the entire spectral regions follow the technique described by Liou (1976).

3.2. Solar Radiation

In the solar spectrum, the primary gaseous absorbers considered were water vapor, ozone, molecular oxygen, and carbon dioxide. Note that the CO_2 absorption contribution was overshadowed by water vapor absorption in the near infrared. In addition, scattering and absorption by clouds and aerosols were taken into account. Both absorption and scattering are strongly dependent upon wavelength. In the ultraviolet and visible bands, absorption by ozone in the 0.3 μm and 0.5 μm bands, and by oxygen in the 0.76 μm band is considered.

The range of solar spectrum considered in this research was that from 0.2 to 3.4 μm. The particular bands chosen, the fractional solar flux in each band, and the primary absorber in each band are presented in Fig. 1. The value of the solar constant used in this study was 1353 W m^{-2} (Thekaekara, 1976). The fractional solar flux in each band was also determined from the work of Thekaekara (1974).

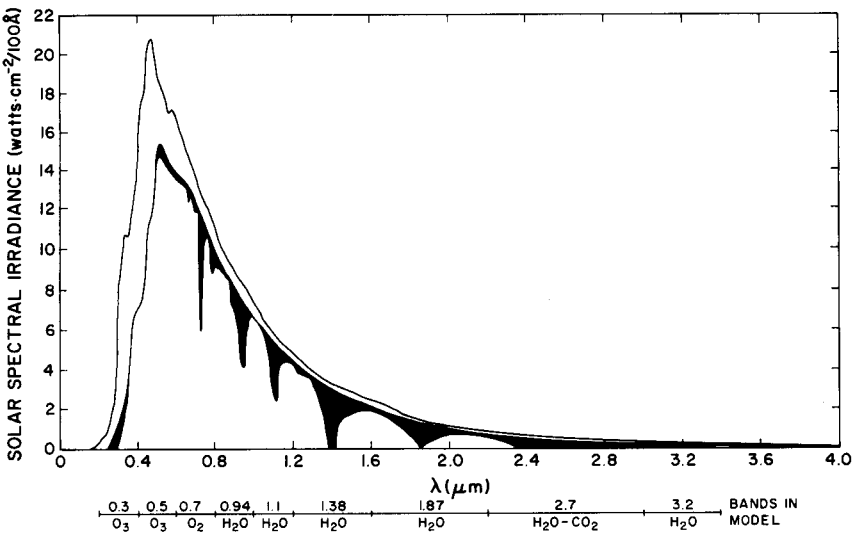

FIG. 1. Spectral energy curve of solar radiation at the top of the atmosphere. The spectral bands utilized in the solar radiation program are indicated. The inner curve is the solar spectrum at the bottom of the atmosphere, and the shaded areas are absorption bands. (After Thekaekara, 1974.)

3.2.1. Water Vapor and Carbon Dioxide Absorption. Water vapor and carbon dioxide absorb solar radiation in the vibrational-rotational bands in the near infrared, most strongly in the 2.7 μm band. The 3.2 μm and the overtone and combination bands in the near infrared also provide significant contributions to the water vapor absorption. A strong absorption band exists at 6.3 μm, but very little solar energy is available in that spectral region, so it was neglected.

Liou and Sasamori (1975) developed a new formula for the mean absorptivity of water vapor and carbon dioxide absorption based upon the empirical formulas derived by Howard *et al.* (1956). It is given by

$$\bar{A} = \frac{1}{R}[C + D \log_{10}(x + x_0)] \tag{10}$$

where $x = uP^{K/D}$, $x_0 = 10^{-C/D}$, C, D, and K are empirical constants, R is the spectral interval for the absorption band, and u is the path length. The new formula is now applicable to both strong and weak absorption.

The continuous function for absorption can now be represented by a series of exponential functions, physically equivalent to spectral subintervals.

$$\bar{A} = 1 - \sum_{m=1}^{M} w_m \exp(-k_m x) \tag{11}$$

where M is the total number of subintervals for each band, w_m the weighting function for each subinterval, k_m the equivalent absorption coefficient for each subinterval, and x has some value between 0 and 300.

After evaluating Eq. (10) for total absorption, Eq. (11) is applied to obtain values for k_m and w_m. For the weak bands, the values of x chosen were 300, 30, 3, 0.3, and 0.03; and for the strong 2.7 μm band, x = 100, 10, 1, 0.1, and 0.01. Once the weights and equivalent absorption coefficients have been determined, water vapor optical depths for each subband and atmospheric layer are computed from

$$\Delta\tau_m^l = k_m \, \Delta x_l, \qquad m = 1, 2, \ldots, M \tag{12}$$

where Δx_l is calculated for an effective atmospheric pressure at layer l by

$$\Delta x_l = u_{l+1} \bar{P}_{l+1}^{K/D} - u_l \bar{P}_l^{K/D}, \qquad \bar{P}_l = \int_0^{u_l} P \, du/u_l \tag{13}$$

3.2.1. Ozone Absorption. Absorption by atmospheric ozone occurs mostly in the ultraviolet portion of the solar spectrum, with weak absorption in the blue side of the visible. In the model, ozone absorption was considered in two spectral bands, 0.3 μm (0.2–0.4 μm) and 0.5 μm (0.4–0.6 μm). The O_3 absorption as a function of altitude is expressed by the atmospheric ozone absorption coefficient given by Elterman (1968) as $\beta_3(Z, \lambda) = A_\nu(\lambda) D_3(Z)$, where β_3 is the atmospheric ozone absorption coefficient (km^{-1}), A_ν is the pure ozone absorption coefficient after Vigroux (1953), D_3 is the ozone equivalent thickness (cm/km), and Z is the height (km). Values of A_ν were given as a function of wavelength. These values were plotted and a representative value of A_ν selected after weighting over the solar flux in each band with an expression

$$A_R = \sum_i A_{Ri} f_{Ri} / \sum_i f_{Ri}$$

where f_{Ri} is the fractional solar flux in each wave number interval. The values of D_3 were taken from McClatchey *et al.* (1972) where values are tabulated against height for all five atmospheres. Once the values for $\beta_3(Z, \lambda)$ have been determined, the ozone optical depth can be calculated from

$$\tau_3(Z, \lambda) = \int_0^Z \beta_3(Z', \lambda) \, \Delta Z' \tag{14}$$

3.2.3. Absorption by Molecular Oxygen. Absorption by O_2 is computed rather simply, since its concentration is uniform in the vertical, given by McClatchey *et al.* (1972) as 0.236 gm cm^{-2}/mb. The oxygen absorption coefficient was obtained by an exponential fit of its absorption curve, after Yamamato (1962), using the same fitting routine as for water vapor. The layer optical depth for oxygen in the 0.76 μm oxygen band was then determined from

$$\Delta\tau_2^l = 0.263 k_2 \, \Delta\bar{p}^l \tag{15}$$

where $\Delta\bar{p}^l$ is the incremental effective pressure for the layer, and k_2 the equivalent absorption coefficient for the oxygen.

3.2.4. Rayleigh Scattering. Molecular scattering cannot be disregarded in the solar spectrum, particularly in the middle layers of the atmosphere below the ozone layer and above the top of the water vapor layer. The Rayleigh scattering optical depth $\Delta\tau_l^R$ for any layer l of geometrical thickness ΔZ may be calculated from

$$\Delta\tau_l^R(\lambda) = \int_{\Delta z_l} \beta^R(\lambda, Z)\, dZ = \sigma^R \int_{\Delta Z_l} N(Z)\, dZ \tag{16}$$

where β^R represents the volume scattering cross section for air molecules, $N(Z)$ the number density of molecules at height Z, and $\sigma^R(\lambda)$ the Rayleigh scattering cross section.

In order to consider simultaneously the effects of molecular scattering and absorption, the single scattering albedo for the layer is defined by

$$\tilde{\omega}_0^R = \frac{\Delta\tau_l^R}{\Delta\tau_l^R + k_m \, \Delta x_l}, \qquad m = 1, 2, \ldots, M \tag{17}$$

The normalized phase function for Rayleigh scattering is given by the well-known expression $P^R(\theta) = \frac{3}{4}(1 + \cos^2\theta)$, where θ is the scattering angle. The total optical depth for a Rayleigh layer is given by

$$\Delta\tau_l = \Delta\tau_l^R + k_m \, \Delta x_l, \qquad m = 1, 2, \ldots, M \tag{18}$$

In a similar manner, absorption due to ozone and molecular oxygen can be taken into account.

3.2.5. Aerosol Scattering and Absorption. The atmospheric aerosol model used in this research was that of a light background concentration providing about 23-km surface visibility (Elterman, 1968). The particular aerosol utilized is a water-soluble particle with refractive indices as given by Shettle and Fenn (1975). The size distribution assumed was a modification of the bimodal log-normal distribution given by Shettle and Fenn (1975).

For spherical aerosol particles, the single scattering albedo properties may be derived from the exact Mie solution with the known information concerning the size and refractive indices. A Mie scattering program was run to obtain aerosol phase functions and scattering and absorption cross sections σ_s^A and σ_a^A, by spectral band. The optical depths due to scattering and absorption by aerosols were then computed from

$$\Delta\tau_s^A = \Delta Z_l \int_{\Delta r} \sigma_s^A(\lambda, r) n(r)\, dr \tag{19}$$

for scattering, and

$$\Delta\tau_a^A = \Delta Z_l \int_{\Delta r} \sigma_a^A(\lambda, r) n(r)\, dr \tag{20}$$

for absorption, where ΔZ_l is the thickness of the aerosol layer, σ_s^A and σ_a^A are the scattering and absorption cross sections of aerosol particles of radius r, and $n(r)\, dr$ is the number of aerosols per unit volume within the size range dr.

Using the computed optical depths, and the Mie phase functions computed from the Mie scattering program, the single scattering albedos and phase functions for a uniformly mixed volume of aerosols and molecules can be computed, respectively, as follows:

$$\tilde{\omega}_0^{R+A} = \frac{\Delta\tau^R + \Delta\tau_s^A}{(\Delta\tau^R + \Delta\tau_s^A) + (\Delta\tau_a^A + k_m \Delta x_l)} \tag{21}$$

and

$$P^{R+A}(\theta) = \frac{\Delta\tau_s^A P^A(\theta) + \Delta\tau^R P^R(\theta)}{\Delta\tau_s^A + \Delta\tau^R} \tag{22}$$

3.2.6. Cloud Absorption and Scattering. The effects of clouds on the transfer of solar radiation are determined by the particle phase (liquid water or ice), concentration, size, and size distribution. These factors combine to determine the single scattering albedo and phase function. The cloud thickness is also an important parameter in determining the absorption, reflection, and transmission of radiation by the individual cloud. Finally, the spatial and temporal distributions of clouds and the different cloud types are very important considerations in determining the effects of the clouds upon the radiation balance of the Earth–atmosphere system and consequently upon the general circulation and climate.

For the purposes of this model, clouds were divided into six types with the cloud parameters given by Liou (1976). Note that cirrus clouds are assumed to be composed of cylinders 200 μm in length and 30 μm in radius. The single scattering properties of clouds were determined much

as described previously for gases and aerosols. The absorption optical depth for cloud water vapor is determined from Eq. (12).

The scattering programs for spheres and long cylinders (Liou, 1973b) were also run to obtain values of the phase function and the volume scattering and absorption cross sections for the different cloud types by spectral band. Spectral-dependent refractive indices for water and ice are taken from Hale and Querry (1973) and Schaaf and Williams (1973), respectively. The phase function and single scattering albedo for an atmospheric layer containing molecules, aerosols, and clouds are given by

$$P^{R+A+C}(\theta) = \frac{\Delta\tau_s^A P^A(\theta) + \Delta\tau_s^C P^C(\theta) + \Delta\tau^R P^R(\theta)}{\Delta\tau_s^A + \Delta\tau_s^C + \Delta\tau^R} \tag{23}$$

$$\tilde{\omega}_0^{R+A+C} = \frac{\Delta\tau^R + \Delta\tau_s^A + \Delta\tau_s^C}{(\Delta\tau^R + \Delta\tau_s^A + \Delta\tau_s^C) + (\Delta\tau_a^A + \Delta\tau_a^C + k_m \Delta x_l)} \tag{24}$$

where superscript C denotes radiative properties of clouds.

The geometrical properties of the cloud that are of interest in the model include its thickness and horizontal extent. All clouds, for the purposes of the radiative transfer calculations, are considered to be of infinite horizontal extent and plane parallel. After the transfer calculations and heating rate computations have been performed, the fractional cloudiness of each type by season and latitude is considered. Similarly, cloud thickness is a function of type, season, and latitude. The radiative properties of the cirrus clouds considered are presented in Table I.

3.2.7. Solar Zenith Angle. The duration of sunlight and the zenith angle of the Sun are important parameters in determining the radiation balance of the Earth–atmosphere system. The zenith angle of the Sun is computed from the equation

$$\sin\alpha = \sin\phi \sin\delta + \cos\phi \cos\delta \cos h \tag{25}$$

where α is the altitude of the Sun (angular elevation above the horizon), ϕ the latitude of the observer, δ the declination of the Sun, and h the hour angle of the Sun. The solar zenith angle is then given by $\theta = 90° - \alpha$, and more commonly, the cosine of the zenith angle, $\mu_0 = \cos\theta$.

In general, the solar zenith angle varies significantly each hour during the day. The one exception is the arctic summer. Sunlight duration varies with season and latitude.

The vertical resolution of the model atmosphere varied according to spectral band and cloud structure. In the solar band, 15 layers were used, with their thicknesses varied to resolve better the clouds and lower layers

TABLE I. SINGLE SCATTERING ALBEDO $\tilde{\omega}_0$ AND VOLUME EXTINCTION COEFFICIENT β_{ext} OF ICE CYLINDERS FOR SOLAR AND INFRARED BANDS

Band (μm)	$\tilde{\omega}_0$	β_{ext} (km^{-1})
0.3 0.5 0.7	1.0	1.141
0.94 1.1 1.37	0.999	1.141
1.87	0.783	1.280
2.7 3.2	0.524	1.259
6.3	0.511	2.082
9.6	0.531	1.437
10	0.520	1.387
15	0.527	1.467
20	0.554	1.556

of the troposphere. In the terrestrial infrared band, 100 layers were utilized. Within the thermal IR bands, layer thicknesses were kept constant.

The computations for the solar radiation portion of the radiation budget began with execution of a program to establish the profiles of atmospheric quantities such as water vapor path length, as functions of atmosphere type and cloud case. Optical depths for gaseous absorption, aerosol scattering, and cloud scattering and absorption were then computed for each spectral subinterval and for every layer for the particular atmosphere–cloud type case. Phase functions for the Rayleigh atmospheres and the combination of Rayleigh only, cloud and Rayleigh, aerosol and Rayleigh, and cloud, aerosol, and Rayleigh were computed. Single scattering albedos were similarly computed for each case and layer. A routine to expand the phase function in Legendre polynomials was then employed, and the basic input data for the transfer program were then available.

The transfer program computed the intensities, fluxes, and heating

rates for each cloud type–atmosphere case for values of $\mu_0 = 0.01$, 0.2, 0.4, 0.6, 0.8, and 1.0 at each of three surface albedos for each atmosphere. The surface albedos were chosen to span the range of values of zonally averaged A_s encountered within the particular atmosphere–season case.

3.3. Terrestrial Thermal Radiation

The requirements for terrestrial infrared radiation calculations differ somewhat from those for solar radiation. For thermal radiation there is no dependence upon astronomical parameters or upon the Earth's surface albedo. Instead, the temperature structure of the atmosphere must be well described, the calculation of transmittances using the Goody random model must be thoroughly thought out, and the generation of boundary conditions within the cirrus clouds must be dealt with in great detail.

3.3.1. Gaseous Absorption in the Infrared. In the terrestrial spectrum, the primary gaseous absorbers are water vapor, carbon dioxide, and ozone. Figure 2 (after Roewe and Liou, 1978) shows the terrestrial spectrum as obtained by satellite, superimposed on plots of the spectral distribution of thermal emission for a number of Earth-like temperatures.

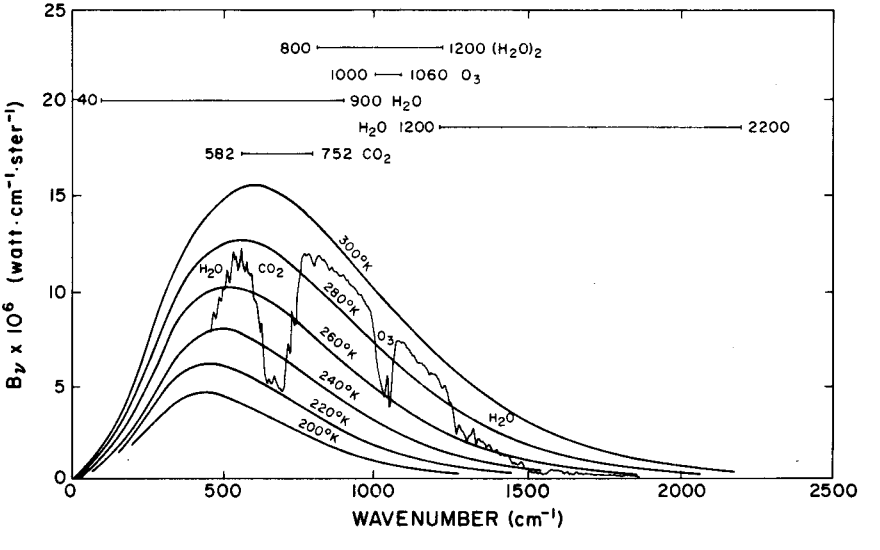

FIG. 2. Terrestrial infrared spectrum and spectral bands. An emission spectrum taken by the IRIS instrument over the tropics is also shown. (After Roewe and Liou, 1978.)

The primary absorption bands, the 15 μm CO_2 band, the 9.6 μm O_3 band, and the water vapor vibrational–rotational band are labeled on the plot.

The Goody random band model was used to compute flux transmissions in all infrared spectral bands except the water vapor continuum band. The Goody model (Goody, 1964) approximates the real spectrum by assuming that spectral lines are randomly distributed within the band and that intensities are distributed exponentially. Assuming a Lorentz line shape, the transmission over a spectral interval R may be given by

$$T_R(u) = \exp\left[-\frac{S_0 u}{\delta}\left(1 + \frac{S_0 u}{\pi\alpha}\right)^{-1/2}\right] \tag{26}$$

where δ is the mean line spacing, S_0 is the mean line intensity, α the line half-width, and u is the absorber amount. For a given u, the transmission function reduces to an expression involving the two parameters S_0/δ and $S_0/\pi\alpha$ (Rodgers and Walshaw, 1966). For ozone, the statistical band parameters determined by Goldman and Kyle (1968) were used.

For the water vapor continuum empirical model, parameters determined by Roberts *et al.* (1976) were employed. The overlap in this band with the 9.6 μm ozone band was not important, since the ozone absorption was restricted to the stratosphere while the continuum absorption was only important below 6–8 km.

The pressure variation over a vertical transmission path through the atmosphere is accounted for by the Curtis-Godson approximation, wherein the transmission of an atmospheric path may be approximated by the transmission of a constant pressure path with absorber amount and weighted line half-width $\bar{\alpha}$. The flux transmission between any two levels Z_1 and Z_2 with a path length u for a spectral interval r is given by $T_R^r(u) = T_R(1.66u)$.

3.3.2. Flux Calculations in the Clear Atmosphere. For a clear, nonscattering, plane parallel atmosphere in local thermodynamic equilibrium, the following equations (Rodgers and Walshaw, 1966) describe the upward and downward directed spectral fluxes at some arbitrary level Z;

$$F_R^{\uparrow}(Z) = T_R(Z, 0)[\pi B_R(g) - \pi B_R(0)] + \pi B_R(Z) - \int_0^Z T_R(Z, Z')\frac{d\pi B_R(Z')}{dZ'}\,dZ' \tag{27}$$

$$(28)\quad F_R^{\downarrow}(Z) = T_R(Z, Z_T)[\pi B_R(Z) - \pi B_R(t)] - \pi B_R(Z) - \int_Z^A T(Z, Z') \frac{d\pi B_R(Z')}{dZ'} dZ'$$

where $\pi B_R(t)$ denotes the downward flux at the top of the atmosphere, $\pi B_R(g) - \pi B_R(0)$ accounts for the temperature discontinuity at the ground, and A is the uppermost level to be considered in computing fluxes.

The flux transmittances in the atmosphere are computed by dividing the infrared spectrum into bands sufficiently narrow for the Planck function to be regarded as constant within the band. The Goody random band model is then applied to the various bands, with the exception of the water vapor continuum. In the continuum, empirically determined transmittances were used.

In the presence of a black cloud layer, Eqs. (27) and (28) must be modified to account for the emission by the cloud top and bottom. With the cloud present, the upward flux above the cloud top must be represented by

$$(29)\quad F_R^{\uparrow}(Z) = F_R^{\uparrow}(Z_{CT})T_R(Z, Z_{CT}) + \pi B_R(Z) - \pi B_R(Z_{CT})T_R(Z, Z_{CT}) - \int_{Z_{CT}}^{Z} T_R(Z, Z')\, d\pi B_R(Z')$$

if no temperature discontinuity is present at the cloud top. Likewise, if there is no temperature discontinuity at the cloud bottom, the downward flux below the cloud base can be expressed by

$$(30)\quad F_R^{\downarrow}(Z) = F_R^{\downarrow}(Z_{CB})T_R(Z, Z_{CB}) - \pi B_R(Z) + \pi B_R(Z_{CB})T_R(Z, Z_{CB}) - \int_{Z}^{Z_{CB}} T_R(Z, Z')\, d\pi B_R(Z')$$

In these two equations, Z_{CT} and Z_{CB} are the heights of the cloud top and base, respectively. Note that the upward fluxes below the cloud and the downward fluxes above the cloud top are unaffected by the presence of the cloud.

3.3.3. Radiative Transfer in the Presence of Cirrus. The optically thin cirrus clouds considered in the present study require the more detailed computation of radiant intensities from which flux values may be derived. This is because the scattering by cloud particles must be considered. Likewise, in the aerosol layer, scattering and absorption by the aerosols require the analytic computations of the radiative transfer. For these

reasons, the discrete-ordinates method described previously must be employed in the longwave spectrum. The solution for the radiative transfer for thermal radiation in cloudy atmospheres has been described previously.

The generation of the boundary conditions in the infrared transfer case is a slightly different problem from that of developing the boundary conditions in the solar spectrum (Liou, 1974b). To compute the necessary boundary conditions, clear atmosphere transmittances above and below the cloud were generated from the model parameters given earlier. The resultant transmission profiles were then approximated with a summation of exponentials, such that

$$T_R(u) \cong \sum_{m=1}^{M} w_m e^{-k_m u} \tag{31}$$

where the w_m and k_m are weights and equivalent absorption coefficients and M is the number of terms required to achieve sufficient accuracy.

Thus it can be seen that this procedure very closely resembles the procedure for approximating water vapor absorption in the solar spectrum. In the infrared bands, the w_m and corresponding k_m are assigned to the spectral subintervals such that the largest k_m is assigned to the region of the band with strongest absorption. The width of the spectral subband is then equal to w_m.

The transmission for each angle is given by

$$T_{Rm}(u/\mu_i) = \exp(-k_m u/\mu_i), \qquad m = 1, \ldots, M \tag{32}$$

where T_{Rm} is the transmission for the mth subinterval of the spectral band R at angle μ_i. Once these transmittances have been calculated, the upwelling intensities into the cloud base are computed for the spectral subinterval by

$$I^{\uparrow}_{Rm}(Z_b, \mu_i) = B_{Rm}(T_s)T_{Rm}(Z_b, \mu_i) + \int_0^{Z_b} B_{Rm}[T(Z')] \frac{dT_{Rm}(Z', \mu_i)}{dZ'} dZ' \tag{33}$$

and the downwelling intensities into the cloud top from

$$I^{\downarrow}_{Rm}(Z_t, -\mu_i) = \int_{Z_T}^{\infty} B_{Rm}[T(Z')] \frac{dT_{Rm}(Z', -\mu_i)}{dZ'} dZ' \tag{34}$$

With the necessary boundary conditions now available, a set of linear equations similar to Eqs. (3)–(5) can now be solved for the unknown coefficients L_j. It follows that fluxes can be computed for each layer and spectral subinterval. When the fluxes are summed over the subintervals

of each band and then summed over bands, net fluxes are computed for each layer, and from these are derived the cooling rates as outlined in Section (3.1).

Since the spectral subintervals determined from the exponential fitting within the cloud do not necessarily match the subintervals in the Goody model, the fluxes from each component cannot be added. Therefore, the fluxes emerging from the cloud top and bottom are attenuated to each level in the atmosphere above and below the cloud with the expressions

$$F_m^{\uparrow}(Z) = F_m^{\uparrow}(Z_{CT}) \exp(-1.66 k_m \Delta u) \tag{35}$$

$$F_m^{\downarrow}(Z) = F_m^{\downarrow}(Z_{CB}) \exp(-1.66 k_m \Delta u) \tag{36}$$

so that at each level in the atmosphere the cloud contribution is thus the sum of the M subinterval fluxes of Eqs. (35) and (36). The total band fluxes derived from summation of the Goody subintervals may now be combined with the band fluxes from the cloud to produce the total band fluxes at each level outside the cloud.

The inclusion of aerosol radiation contribution is similar to that in the solar spectrum. We found that the light aerosol concentration is significant only in the window region.

4. Heat and Radiation Budgets of the Atmosphere

4.1. Climatology Data

The bulk of the data required for zonally averaged global radiation computations involving cirrus includes atmospheric profiles, cloud parameters, and surface albedo (reflectivity). The atmospheric profiles used were taken from the report by McClatchey *et al.* (1972) who compiled the water vapor, ozone, pressure, density and temperature profiles for tropical (0°–30°), midlatitude (30°–60°), and arctic (60°–90°) atmospheres. The atmospheric profiles are given for both winter and summer seasons. The concentrations of the uniformly mixed gases of interest, CO_2 and O_2 were taken to be 5.11×10^{-4} and 0.236 gm cm^{-2}/mb, respectively, constant with season and latitude. Values of surface albedo for the northern hemisphere were taken from the work of Katayama (1967b) and adopted from Sasamori *et al.* (1972) for the southern hemisphere.

The atmospheric profiles used may not be truly representative of both northern and southern hemispheres, since no accounting is made for interhemispheric differences of water vapor, ozone, and temperatures arising from the differences in geography between the two hemispheres.

Also, the use of only three profiles to represent a hemisphere for a given season causes a lack of latitudinal resolution. However, compact climatological summaries of zonally averaged atmospheric profiles are not available for both hemispheres. Furthermore, the effects of clouds tend to dominate the radiation budget, overshadowing the variation due to atmospheric differences. Thus, the 10° latitudinal resolution of the cloud climatologies used offsets, at least partially, the lack of resolution in the model atmospheres.

Clouds were divided into six types, which include (1) high clouds (Ci, Cs, Cc); (2) middle clouds (As, Ac); (3) low clouds (St, Sc); (4) cumulus (Cu); (5) cumulonimbus (Cb); and (6) nimbostratus (Ns). The fractional cloud cover for each cloud type as a function of the latitude will be taken from Telegadas and London (1954) for the northern hemisphere. In their report, the cloud base heights for six types were also given as functions of the latitude, along with the top heights for Cu, Cb, Ns, and middle clouds. As for low and high clouds, the mean cloud thicknesses provided by Katayama (1966) were employed. Cloud data for the southern hemisphere were obtained from the table provided by Sasamori *et al.* (1972). Cloud and aerosol parameters used were described in the previous section.

4.2. Solar Heating

The broad-scale features of the planetary climate are determined by the distribution of solar radiation over the globe. The differential heating of the equatorial and polar regions, in addition to providing the ultimate energy source for the Earth's general circulation, is also responsible for causing the climatic extremes between the tropical and polar latitudes, although the effects of direct solar insolation are mitigated to a great degree by the effects of the general circulation.

In previous radiation budget models, the solar radiative flux calculations have been carried out through the use of parameterized empirical equations and the details of scattering by clouds and aerosols largely overlooked. In the present model, calculations of the optical depths and single scattering parameters were carefully carried out for the full range of the solar spectrum containing significant amounts of energy. The discrete-ordinates method was employed to perform the extensive calculations necessary for a full investigation of the solar energy spectrum and its effects upon the heat balance of the Earth's atmosphere.

The net effect of solar radiation upon the atmosphere is, of course, to warm the atmosphere and Earth everywhere. Every portion of the Earth

in sunlight receives energy from the Sun and is warmed to a greater or lesser degree. The primary factors that determine the degree of solar warming received by a particular region on the average are, most importantly, the cloud cover of the region and the latitude of the region, which determines the range of solar zenith angles experienced by the area. Other factors are the annual range of surface albedos, the presence of aerosols in greater or lesser concentrations, and the water vapor and ozone contents of the atmosphere.

The zonally averaged profiles of the solar heating rate at the representative latitudes of 15°, 45°, and 75°N are illustrated in Fig. 3 for the months January and July. In the figure, the maximum solar heating of about 2.2°C/day is observed in the summer hemisphere tropical and subtropical regions. Second maxima occur in the troposphere in the summer polar regions. These are about 1.5–2.0°C/day and are accounted for by the duration of daylight in these regions as well as by the occurrence of a maximum of cloudiness in the subarctic summer. Minima occur in the upper troposphere and lower stratosphere in both months. Generally, there is a lack of both clouds and absorbing gases at these altitudes, leading to heating rates of only about 0.02 to 0.04°C/day. Maxima again occur in the upper stratosphere, above 25 km, due almost exclusively to the presence of ozone. The heating produced is on the order of 1.5 to 1.8°C/day and is an important source of heating for the atmosphere. Effects of aerosols appear to increase the heating rate in the atmosphere. Latitudinal cross sections of zonally averaged solar heating for January are shown in Fig. 4. These cross sections were constructed using the climatological cloud and surface conditions applied at 10° latitude intervals and three atmospheric profiles.

4.3. Thermal Cooling

While the radiation from the Sun warms the Earth's atmosphere everywhere, the role of terrestrial infrared radiation is more complex. In the main, the thermal radiation serves to cool the atmosphere, radiating away to space energy equivalent to the solar input, maintaining the radiative balance. Under certain conditions, however, thermal radiation adds to the warming of the atmosphere at particular levels and locations, essentially acting as another mechanism for converting solar energy to heat in the atmosphere.

The global distribution of thermal radiation is somewhat easier to model than the solar radiation, since there is no surface albedo or diurnal, seasonal, and latitudinal zenith angle dependence to be dealt with. In the

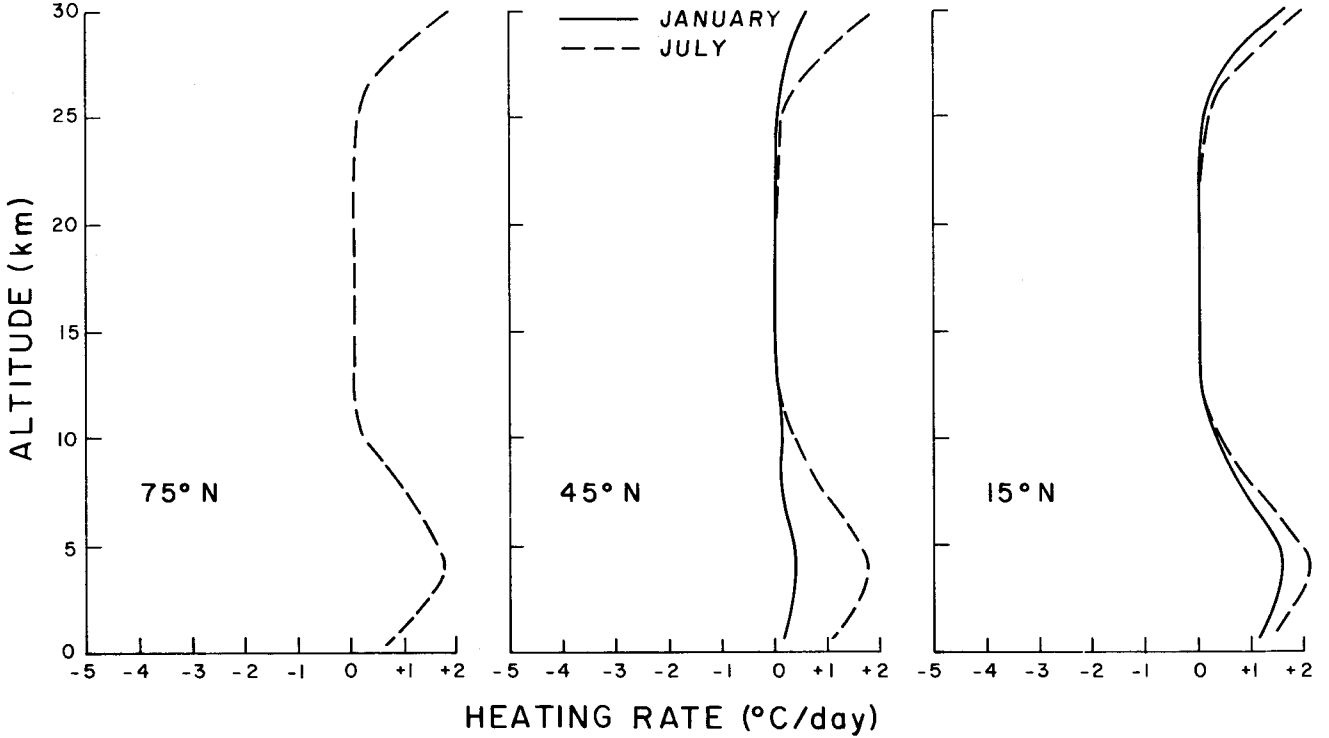

FIG. 3. Solar radiative heating profiles at three latitudes for January and July conditions.

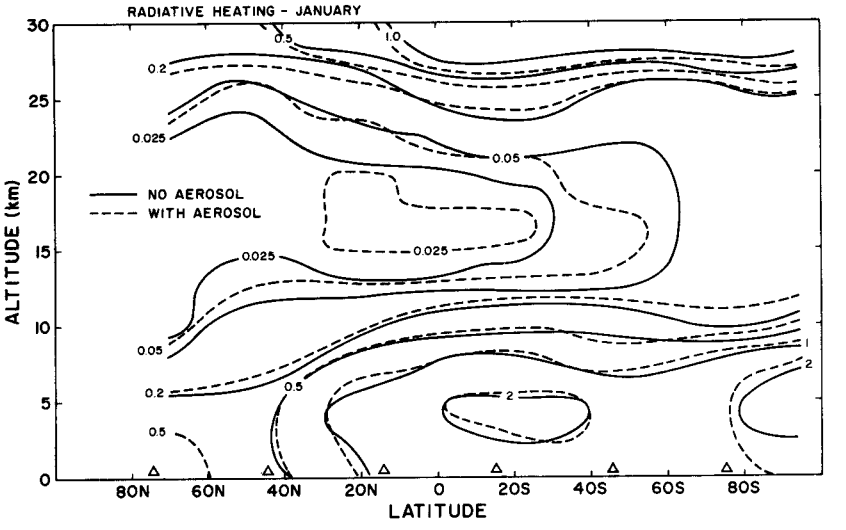

FIG. 4. Latitudinal cross sections of zonally averaged solar radiative heating (°C/day) of the atmosphere for January. The symbol △ represents the latitudes at which the atmospheric profiles were used (see text for explanation).

present model, the seasonal and latitudinal variations of the infrared radiation budget are determined only by the particular atmospheric profile used and by the seasonal and latitudinal variations of clouds.

The zonally averaged cooling profiles for January and July, at 15°, 45°, and 75°N, are presented in Fig. 5. The maximum cooling occurs in the summer stratosphere, due exclusively to ozone and CO_2. Indeed, almost all cooling above the tropopause is due to these two gases, since the water vapor profiles are cut off at 16 km in the model. Ozone is also responsible for the obvious region of thermal heating found above the tropopause in tropical and subtropical latitudes for both seasons. This heating is associated with the large vertical gradients of ozone concentration and the increase of ozone concentration with height, resulting in a convergence of flux into the region. The heating in this region is supplemented by a similar region of heating due to CO_2 at the tropical tropopause, resulting from the higher temperatures found both above and below the tropopause. In the stratosphere, cooling occurs in relation to the seasonal distribution of ozone concentration and the temperature field and its interaction with the ozone and CO_2 profiles, producing seasonally symmetrical cooling fields.

Water vapor acts to cool the clear atmosphere everywhere since there is an increase of flux with height as the water vapor concentration drops

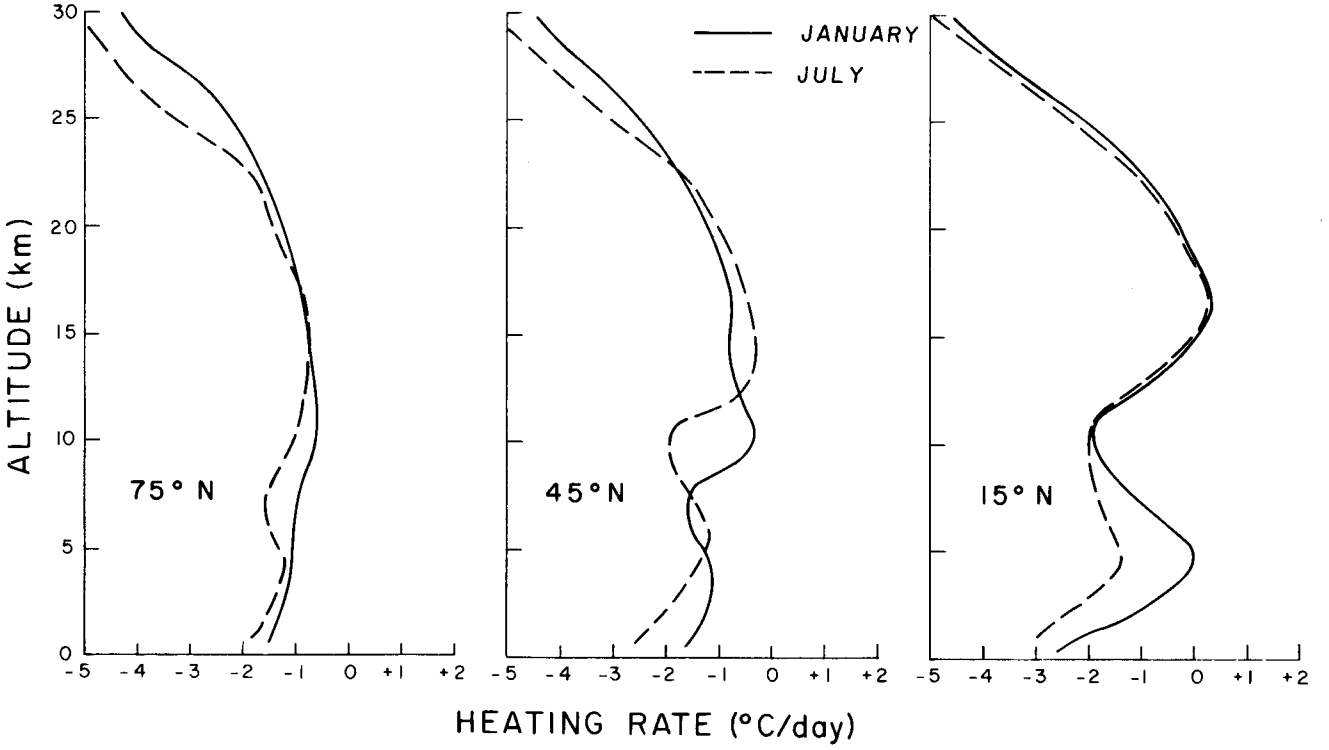

FIG. 5. Thermal radiative cooling profiles at three latitudes for January and July conditions.

off. A secondary maximum of cooling occurs in tropical latitudes within the troposphere which is associated with the large vertical gradients of water vapor and temperature. The effects of clouds are also included in this region, since clouds tend to increase the cooling above their tops and decrease the cooling below their bases. In the vicinity of the tropopause, water vapor exhibits a minimum of cooling in the tropics, again due to the warmer temperatures above and below the tropopause and the resulting convergence of thermal flux into the area. Above the tropopause, very little cooling results from water vapor, only on the order of −0.2°C/day or less, since little water vapor exists there. Near the surface, below 4 km, another maximum of cooling occurs in the tropics and summer midlatitudes, due again to water vapor and temperature gradients. This cooling is offset somewhat by the decrease in the cooling below the cloud bases.

With the cooling rate profiles and fluxes calculated for each atmosphere and cloud type combination, the only tasks left to establish the zonally averaged meridional cooling profiles similar to those of the solar radiation were to interpolate the individual cooling profiles to common atmospheric levels, and then for each latitude, to multiply the individual cloud-type profiles for the appropriate atmosphere by the fractional cloudiness at that latitude. The individual cloud profiles, including the clear column profiles, were then summed at each latitude, and the two seasonal cooling rate cross sections were established. Latitudinal cross sections of zonally averaged infrared cooling for January are shown in Fig. 6.

In summary, the net thermal cooling is dominated by water vapor below the tropopause with maximum cooling, on the order of −2.0°C/day occurring in low latitudes near 10 km altitude. Another maximum at the surface, of about −2.0 to −3.0°C/day, and within the same latitude belt, is also due to water vapor. At the tropical tropopause there exists a relatively uniform level of heating, on the order of 0.3°C/day, resulting from the interactions of CO_2, water vapor, and clouds. Above the tropopause, the thermal cooling effects are due to ozone and CO_2. Above that region there exists steadily increasing cooling toward the summer hemisphere in the upper stratosphere, where cooling on the order of −5.6°C/day is found.

4.4. The Net Heat Budget

The net heat budget was computed by summing the heating and cooling rates presented earlier for each month at each latitude and atmospheric layer. The total heating plots for the two months at the representative

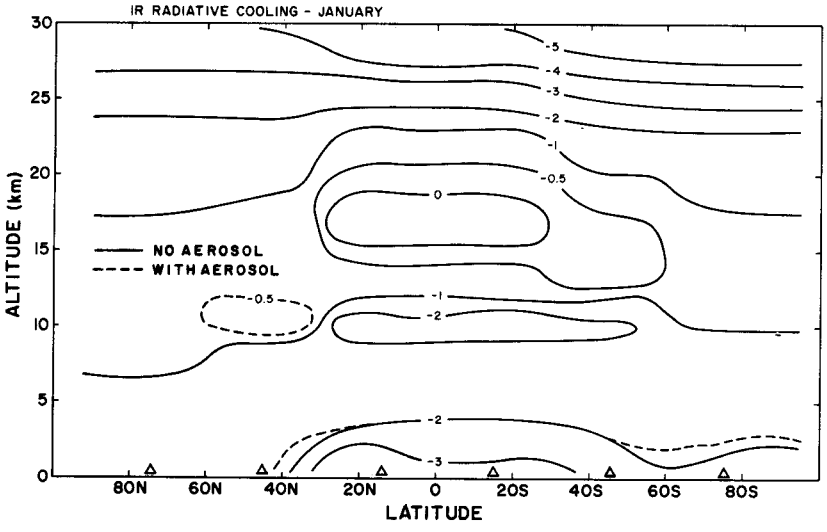

FIG. 6. Latitudinal cross sections of zonally averaged thermal radiative cooling (°C/day) of the atmosphere for January. The symbol △ represents the latitudes at which the atmospheric profiles were used (see text for explanation).

latitudes are presented in Fig. 7. Radiative cooling dominates the solar heating almost everywhere. In the upper stratosphere, above 25 km, intense cooling due to O_3 and CO_2 is found. The thermal cooling of −4 to −5°C/day completely overshadows the solar heating by ozone to produce net cooling of −4 to −4.5°C/day. The large cooling is due, in part, to the effect of clouds. At the tropical tropopause, near 18 km, is found a maximum of longwave heating of about 0.35°C/day. This occurs in the region of minimum solar heating, about 0.025°C/day, to produce net heating. The thermal heating in this region is due to the much higher temperatures above and below the tropopause resulting in a strong flux convergence into the tropopause region. Below this region of heating is a region of maximum cooling, with values near −2.0°C/day. This region is associated with large vertical gradients of water vapor and temperature.

It is apparent from the plots of radiative heating presented in Fig. 5 that cooling by longwave radiation outweighs solar heating at every latitude for both seasons. The cooling is due primarily to water vapor, and is thus a maximum in the tropics. The presence of clouds tends to moderate the cooling in the lower levels of the atmosphere, by reducing the cooling below their bases and producing strong solar heating at their tops. Their effect varies with latitude and season, as the cloud distribution varies.

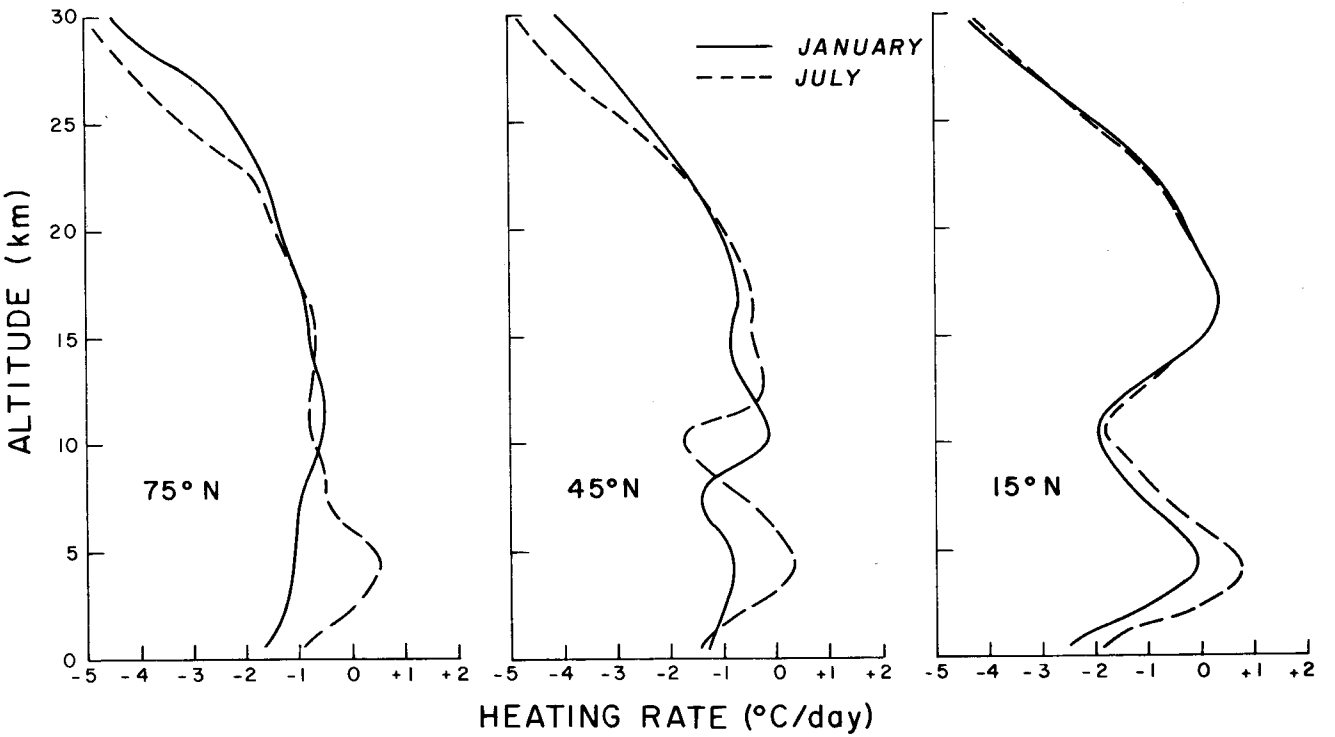

FIG. 7. Net radiative heating profiles at three latitudes for January and July conditions.

Latitudinal cross sections of zonally averaged net radiative heating for January are presented in Fig. 8. Note again that although these cross sections are constructed from the three atmospheric profiles, they do contain cloud information with a 10°C resolution, and it is the cloud field that determines the large-scale features of the heat budget. In reference to Fig. 8, the moderately strong tongue of net heating, extending from the summer pole into the tropical latitudes of the winter hemisphere, at a level of about 5 km, is due to strong water vapor absorption in the near infrared augmented by solar geometry. Heating by clouds also contributes to this feature. The solar heating at the cloud tops is partially offset by the increased thermal cooling above the clouds, but below the cloud bases the heating is supplemented by the reduced thermal cooling. The maximum heating is found in this region near the summertime pole where the length of the period of solar heating offsets the low zenith angle of the Sun. Longwave cooling in this region at a height of 4–5 km is relatively small, due to the low temperatures and the cloud effects. In both hemispheres are found cooling maxima of about −2.0°C/day in the surface layer of the winter tropics. This cooling is due to the water vapor concentration maxima in the surface layer and to a relative minimum of cloudiness in the wintertime tropics as compared with the summer hem-

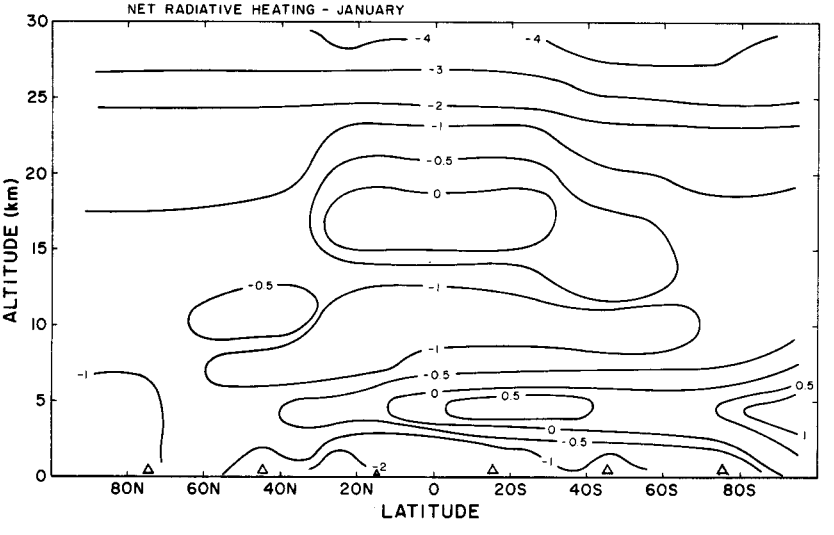

FIG. 8. Latitudinal cross sections of zonally averaged net radiative heating (°C/day) of the atmosphere for January. The symbol △ represents the latitudes at which the atmospheric profiles were used (see text for explanation).

isphere tropics. These plots agree well with earlier work by Dopplick (1972), London (1957), and others, at least in the gross features.

The effects of light background aerosols upon solar heating are demonstrated in Fig. 9, for January and July at the latitude 45°N. As can be seen, the aerosol concentration produces slight additional heating in the lower 10–12 km of the atmosphere. This additional heating is generally on the order of +0.1°C/day. This very light concentration has only little effect upon the heat budget. In the case of thermal cooling, the only detectable effects were in the middle and high latitudes of the summer hemispheres, where a slight increase in cooling, on the order of −0.1–0.2°C/day was computed. Aerosol effects were noticeable only in the window region of the thermal IR spectrum.

4.5. The Radiation Budget

The radiation budget of the Earth–atmosphere system, in terms of the vertical fluxes of solar and longwave radiation, is presented in Tables II

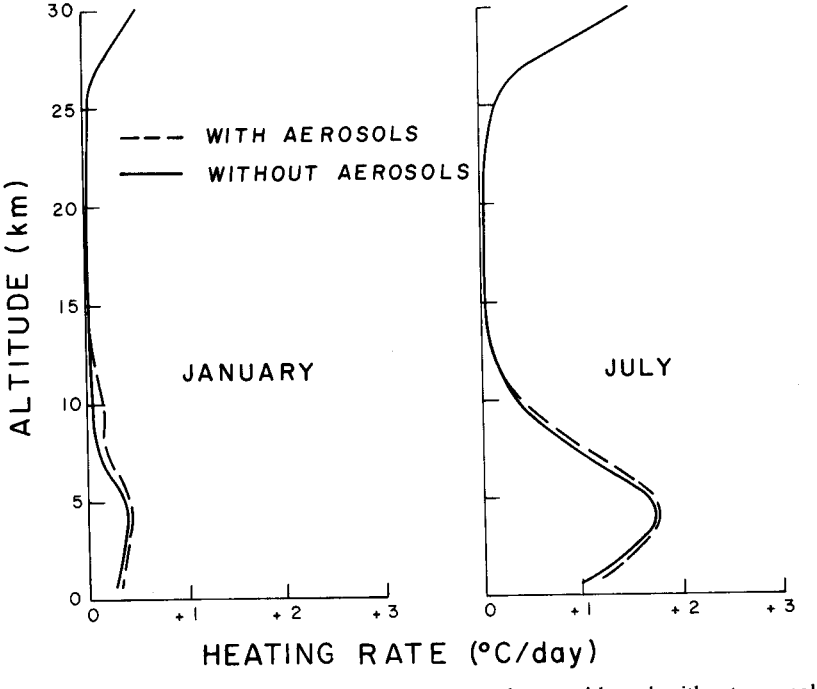

FIG. 9. Comparison of solar heating in the atmospheres with and without aerosols at 45°N latitude for January and July conditions.

TABLE II. GLOBAL SOLAR RADIATION BUDGET (IN UNITS OF ly min^{-1}) FOR JANUARY FOR AN ATMOSPHERE BOTH WITH AND WITHOUT AEROSOL

	Latitude					
January	75°N	45°N	15°N	15°S	45°S	75°S
Insolation at top of atmosphere	0	.230	.517	.691	.732	.722
Absorption in atmosphere						
With aerosol	—	.059	.112	.193	.173	.148
Without aerosol	—	.061	.109	.175	.165	.141
Absorption by surface						
With aerosol	—	.091	.268	.299	.279	.160
Without aerosol	—	.084	.281	.325	.289	.162
Total absorption by atmosphere and Earth						
With aerosol	—	.150	.380	.492	.452	.310
Without aerosol	—	.145	.391	.500	.454	.303
Reflection at atmospheric top						
With aerosol	—	.080	.137	.201	.282	.412
Without aerosol	—	.085	.127	.191	.272	.419
Zonal mean albedo (%)						
With aerosol	—	.36	.27	.29	.38	.57
Without aerosol	—	.37	.25	.28	.37	.58

through IV, for January and July, respectively, for tropical (15°), midlatitude (45°), and arctic (75°) atmospheres. Basically, the tables are in two portions, one dealing with solar radiation and the manner in which it is apportioned in the atmosphere, and the second concerning longwave radiation and its distribution. For the solar part, the important parameters are the solar insolation at the top of the atmosphere, the absorption of solar radiation in the atmosphere, absorption by the surface, and the reflected flux at the top of the atmosphere. The parameters of interest for the longwave radiation include the upward flux at the Earth's surface, the downward flux from the atmosphere arriving at the surface, the upward flux at the atmospheric top, and the net loss of thermal radiation from the atmosphere.

The solar radiation computer model returned values of reflected, transmitted, and absorbed radiation in terms of percentages of the incident solar flux. These values were interpolated to the appropriate month and latitude in a manner similar to that for the heating rates. The value of the reflected radiation fraction was taken as the planetary albedo for the particular month and latitude, and the absorbed fraction was applied to the incident solar flux at each latitude band to determine the flux absorbed

by the atmosphere. The fractional transmission returned by the model refers to diffuse radiation and cannot be used to calculate the solar flux reaching the ground for absorption, since a direct flux must also be considered. For a nonblack surface, that is for $A_s \neq 0$, the solar flux absorbed by the surface is obtained from $t_s = 1 - \gamma + \alpha$, where γ is the local albedo, and α the absorption of solar radiation within the atmosphere. The values for the fractional solar insolation at the top of the atmosphere for each month and latitude were taken from Sasamori *et al.* (1972) for the southern hemisphere and from London (1957) for the northern hemisphere. Note that the asymmetry in solar flux between the two hemispheres is accounted for by the difference in the Earth–Sun distance between January and July and by the different methods used by the previous investigators. London used the monthly averages for the seasons, while Sasamori *et al.* used the daily flux for the 15th day of the month under consideration.

From the computer model for the thermal radiation, values for the upward fluxes at the atmospheric top and the downwelling radiation at the bottom of the atmosphere were obtained and interpolated in a manner similar to that for the solar parameters for each month at each latitude.

TABLE III. GLOBAL SOLAR RADIATION BUDGET (IN UNITS OF ly min^{-1}) FOR JULY FOR AN ATMOSPHERE BOTH WITH AND WITHOUT AEROSOL

	Latitude					
July	75°N	45°N	15°N	15°S	45°S	75°S
Insolation at top of atmosphere	.621	.664	.645	.464	.187	—
Absorption in atmosphere						
With aerosol	.141	.188	.197	.124	.062	—
Without aerosol	.131	.174	.176	.100	.053	—
Absorption by surface						
With aerosol	.158	.251	.273	.226	.050	—
Without aerosol	.154	.264	.309	.253	.068	—
Total absorption by atmosphere and earth						
With aerosol	.299	.439	.471	.353	.112	—
Wihtout aerosol	.286	.438	.485	.353	.121	—
Reflection at atmospheric top						
With aerosol	.323	.225	.174	.111	.075	—
Without aerosol	.335	.226	.161	.109	.065	—
Zonal mean albedo (%)						
With aerosol	.52	.34	.27	.24	.40	—
Without aerosol	.54	.34	.25	.23	.35	—

TABLE IV. GLOBAL LONGWAVE RADIATION BUDGETS (IN UNITS OF ly min^{-1}) FOR JANUARY AND JULY

	Latitude					
January	75°N	45°N	15°N	15°S	45°S	75°S
Upward flux at surface	.307	.455	.638	.646	.540	.374
Downward flux at surface	.239	.384	.532	.563	.481	.321
With aerosol	.243	.386				.323
Net upward flux at surface	.068	.071	.106	.083	.059	.053
Upward flux at top of atmosphere	.257	.269	.362	.350	.341	.317
Net loss from atmosphere	.189	.198	.256	.267	.282	.264
July						
Upward flux at surface	.475	.586	.667	.622	.508	.296
Downward flux at surface	.408	.512	.571	.533	.442	.250
With aerosol	.411				.445	.255
Net upward flux at surface	.067	.074	.096	.089	.066	.046
Upward flux at top of atmosphere	.299	.330	.339	.363	.280	.251
Net loss from atmosphere	.232	.256	.243	.274	.214	.205

The upward flux at the surface was computed using the surface temperature in the Stefan–Boltzmann law where $F = \sigma T^4$. In this expression, F is the total flux of emitted energy, and σ is the Stefan–Boltzmann constant and equals 8.128×10^{-11} cal cm^{-2} K^{-4} min^{-1}. The temperature, T, is the blackbody temperature of the Earth. The net upward flux at the surface is the difference between the flux emitted by the surface and the downward flux from the atmosphere reaching the surface. This is always a positive quantity since the blackbody emission from the Earth is always greater than the nonblack emission from the cooler atmosphere. The net loss from the atmosphere is then the difference between the upward flux at the atmospheric top and the net upward flux at the surface.

In Tables II and III for the solar radiation budget, values are presented both for an atmosphere with and without aerosols. In every case, at least small differences can be detected between the budget parameters for the two models. The aerosols have two effects upon solar radiation, scattering and absorption; and these two effects have competing impacts upon the heating of the atmosphere. The role of scattering is to increase that portion of the incident radiation which is reflected back to space, thus adding to the local albedo and reducing the energy available for heating. Absorption by aerosols acts to increase the warming of the atmosphere. Both effects act to deny a small portion of the solar insolation to the surface, thus reducing the amount of energy available to warm the Earth's

surface. The surface albedo plays an important role in determining whether or not an increase in aerosol loading will act to increase or decrease the local planetary albedo (Liou and Sasamori, 1975), and the effects of absorption seem to overshadow the scattering effects and thus lead to a decrease in local albedo in the higher latitudes.

These effects of aerosols are reproduced, generally, in the present calculations, wherein it can be seen from Tables II and III that the total absorption by the Earth and atmosphere is increased in the aerosol case. The zonally averaged albedos computed here also show the effects of aerosols, which increase the local albedo in the tropical and subtropical regions while reducing the albedos in the higher latitudes. The individual absorption by the atmosphere and the Earth also bear out the expected results, with increased atmospheric absorption due to aerosols leading to a loss of total energy available for absorption at the surface. Minor departures from this general case occur near the poles and are accounted for by the complex interaction of high surface albedo and low zenith angle.

The average absorption of solar radiation by the atmosphere amounts to about 25% for the aerosol atmosphere and about 23% for the nonaerosol case. The absorption decreases toward the poles, in the annual average, faster than the solar insolation decreases, because of the increasing reflection from clouds at lower zenith angles. Surface absorption drops off toward the poles in a similar manner, but at an even faster rate, due mostly to the increasing surface albedos with latitude, and also due to the decrease of energy available for absorption at the surface. The reflected solar flux increases with latitude despite the large variation of insolation at the top of the atmosphere. This is due to the increase of cloudiness with latitude and to the strongly increasing surface albedo from equator toward the poles.

Using the information in Tables II–IV the net monthly radiation balances for the top of the atmosphere, the surface, and the atmosphere as a whole can be computed, as shown in Table V. The radiation budget for the top of the atmosphere is determined by subtracting the upwelling longwave flux at the top of the atmosphere from the solar radiation absorbed by the Earth and atmosphere. The result, shown in Table V, indicates a net gain of energy at the top of the atmosphere in the tropics and summer hemisphere midlatitudes for both January and July. In the annual case, the gain occurs between 35°N and 35°S with losses poleward of that region. The annual global average is a net loss of 0.023 langleys min^{-1}.

At the Earth's surface, the radiation budget is calculated by subtracting the net upward terrestrial radiation from the solar radiation absorbed by

TABLE V. NET RADIATION BUDGETS (IN UNITS OF ly min^{-1}) FOR THE TOP AND BOTTOM OF THE ATMOSPHERE AND NET RADIATION LOSS FOR THE ATMOSPHERE

	Latitude					
January	75	45	15	15	45	75
Net radiation budget for top of atmosphere	−.257	−.119	.018	.142	.111	−.007
Net radiation budget for surface	−.680	.020	.162	.216	.220	.107
Net radiation loss for atmosphere	−.189	−.139	−.144	−.074	−.109	−.116
July						
Net radiation budget for top of atmosphere	.000	.109	.132	−.010	−.168	−.251
Net radiation budget for surface	.091	.177	.177	.137	−.016	−.046
Net radiation loss for atmosphere	−.091	−.068	−.059	−.150	−.152	−.205
Annual						
Net radiation budget for top of atmosphere	−.128	−.005	.076	.066	−.028	−.129
Net radiation budget for surface	.012	.098	.169	.176	.102	.030
Net radiation loss for atmosphere	−.140	−.104	−.095	−.112	−.130	−.160

the surface. This quantity is positive in all of the summer hemisphere and through about 35° latitude in the winter hemisphere in both months. Annually, there is net gain in the tropics and midlatitudes and net loss from the subarctic regions of the northern hemisphere. In the southern hemisphere, the net gain in the antarctic region is very small and may be within the expected error of these calculations. Globally, the annual mean shows a net gain of 0.094 ly min^{-1}. The negative results in the polar regions are due to high surface albedos and low water vapor contents in the subarctic atmospheres.

By combining the solar radiation absorbed by the atmosphere with the divergence of terrestrial radiation, the net loss in Table IV, the net radiation loss for the atmosphere was computed. In the annual case, there results a net global loss of 0.120 ly min^{-1}. This quantity represents a radiative deficit which must be made up by the transfer of latent and sensible heat to the atmosphere from the Earth's surface if the atmosphere as a whole is considered to be in a steady state energetically, and

if no heat transfer across the equator is considered. Sasamori *et al.* (1972) suggest that about 77% of this deficit is made up by the release of latent heat of condensation in the southern hemisphere, and about 70% in the northern hemisphere. The remainder of the deficit must then be compensated by the transport of sensible heat into the lower layers of the atmosphere from the surface.

The global albedos of the Earth for the months January and July and the annual mean were computed by multiplying the zonally averaged albedos for each latitude by the fraction of the Earth's surface contained within the latitude belt represented by the latitude values tabulated. Five atmospheric profiles and the climatological cloud and surface conditions at 10° latitude intervals were used in the calculations. The global albedo for January was computed to be 0.348 and 0.327 for July. These values were determined for the aerosol case and for the aerosol-free atmosphere; the corresponding values were 0.338 and 0.317 for January and July, respectively. The annual mean global albedo was then 0.338 for the aerosol case and 0.328 for the aerosol-free case. As for the two hemispheres, the southern hemisphere possesses a fractionally higher albedo than does the northern hemisphere, both for winter and summer for the aerosol-laden atmosphere. The situation is reversed in the nonaerosol case, however, where the southern hemisphere albedos are marginally higher than the northern in both seasons. This effect is due both to the nonsymmetric cloud distributions and to the higher surface albedos for the polar regions in the southern hemisphere. The planetary albedo results are summarized in Table VI. The annual global albedo for the aerosol case, 0.338, compares favorably with the results of Vonder Haar and Suomi (1971); where the global albedo was determined to be 0.30, Sasamori *et al.* obtained a value of 0.347 for the southern hemisphere and London computed an albedo value of 0.352, for the northern hemi-

TABLE VI. GLOBAL AND HEMISPHERIC MEAN ALBEDOS

	January	July	Annual
Northern hemisphere			
With aerosol	.346	.317	.332
Without aerosol	.340	.308	.324
Southern hemisphere			
With aerosol	.349	.337	.343
Without aerosol	.335	.326	.330
Global			
With aerosol	.348	.327	.338
Without aerosol	.338	.317	.328

sphere. Raschke and Bandeen (1970) measured an albedo of 0.29 to 0.31 for June and July of 1966 from Nimbus II satellite observations.

4.6. Comparison with Previous Models

In Figs. 10–12 comparisons between the present work and previous models and satellite observations are presented for the solar radiation absorbed by the Earth–atmosphere system, the total upwelling longwave radiation at the atmospheric top, and for the zonal mean albedos. The dots denote the latitudes at which the atmospheric profiles were used. In Fig. 10 the total absorption of solar radiation is plotted for January and July and the annual mean. Comparisons with the work of London (1957) and Sasamori *et al.* (1972) show very good agreement in January and fair agreement in July. Generally, the absorption computed in the present work exceeds the absorption computed by the previous investigators. This can be accounted for by the increased absorption due to aerosols and the effects of scattering by aerosols and clouds, which increase the amount of energy available for absorption, in effect, by increasing the optical path lengths through the atmosphere. The earlier investigators used empirical parameterized expressions for the scattering by clouds and aerosols and not the direct computations from Mie and multiple scattering used in the present work.

On the whole, very good agreement for the annual mean of absorption is obtained between the present calculations and the satellite observations presented by Vonder Haar and Suomi (1971) in which five years of satellite data are analyzed. The largest differences occur in the polar regions, particularly in the northern hemisphere, and most of the difference is accounted for by the departures from reality of the cloud and aerosol distributions used in the model. Differences between the present calculations of absorption and the earlier results of London and Sasamori *et al.* may be accounted for, in part, by the more accurate method of accounting for scattering and absorption by aerosols and clouds. Some portion of the differences may also be due to different ozone models used, which would change the total absorption in the 0.3 and 0.5 μm solar bands.

In Fig. 11 the latitudinal distributions of upwelling longwave flux at the top of the atmosphere are compared. Differences between the calculations performed here and previous work can be accounted for primarily by the different water vapor and temperature distributions used. Additionally, in the case of the northern hemisphere, London gave little

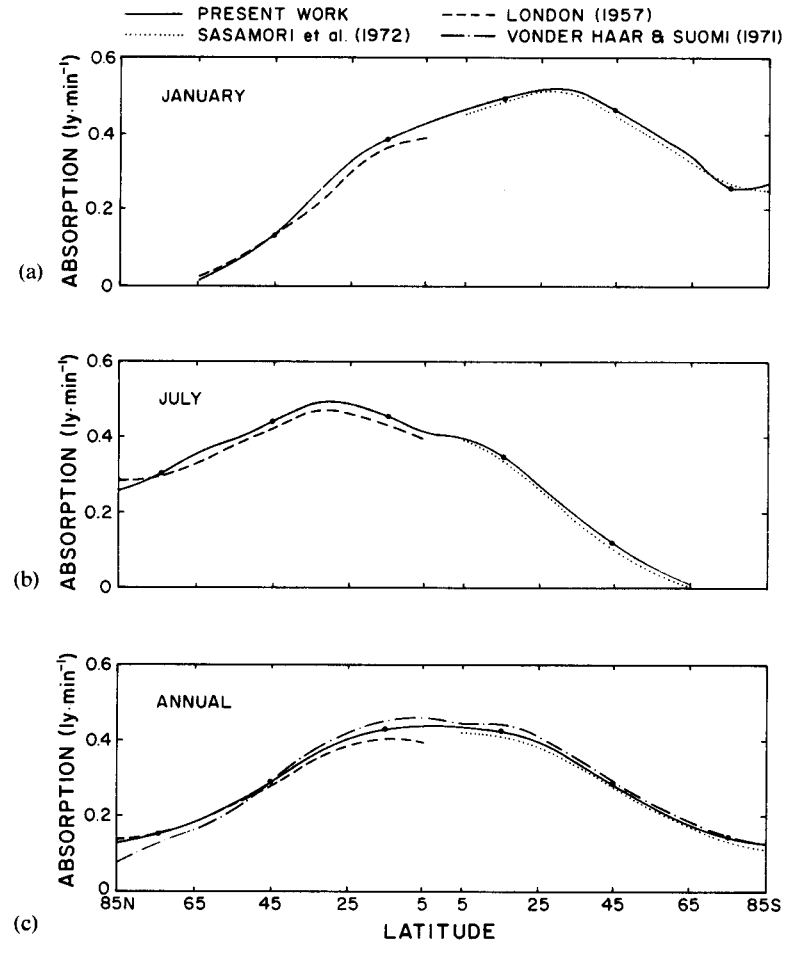

FIG. 10. Absorption of solar radiation by the Earth–atmosphere system: (a) January, (b) July, (c) annual. The dots denote the latitudes at which the atmospheric profiles were employed.

consideration to the role played by ozone in the thermal radiative transfer problem.

On the whole, the present work does an adequate job of reproducing the satellite-observed upwelling longwave flux, except at the poles, where overestimation of the upward flux occurs. The distribution of clouds used in the model may play a significant role in determining the differences between calculated and observed values.

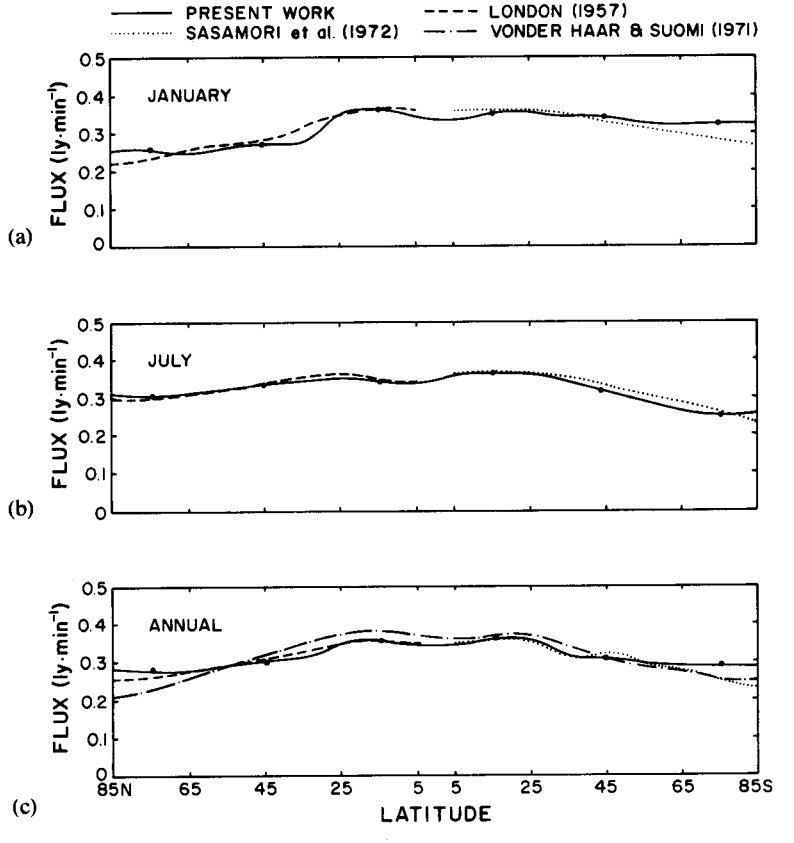

FIG. 11. Total upwelling longwave radiation from the atmospheric top: (a) January, (b) July, (c) annual. The dots denote the latitudes at which the atmospheric profiles were employed.

Finally, the comparisons of planetary albedos are presented in Fig. 12. In the tropics and midlatitudes especially, the present calculations do a better job of reproducing the satellite albedos. In some instances, in the higher latitudes, the present model yields albedos that exceed those of the older works. On the average, all the computed values, both present and past, are larger than the satellite-observed values. In some cases the computed results may exceed the satellite values by as much as 15–20%. Probably the most important reason for the differences is the overestimation of cloudiness, particularly in the tropics. Another factor is the underestimation of absorption in the atmosphere, due to uncertainties and inaccuracies in the treatment of aerosols.

The most comprehensive recent study of atmospheric heating available for comparison with the present work is that of Dopplick (1972). Many of the grosser features of the heating profile are observed in both studies, at least below the tropopause. The areas of net cooling in the tropical and midlatitude troposphere are very similar and, indeed, demonstrate close agreement on the values of the cooling. Dopplick also depicts a tongue of net warming extending from the antarctic toward the equator,

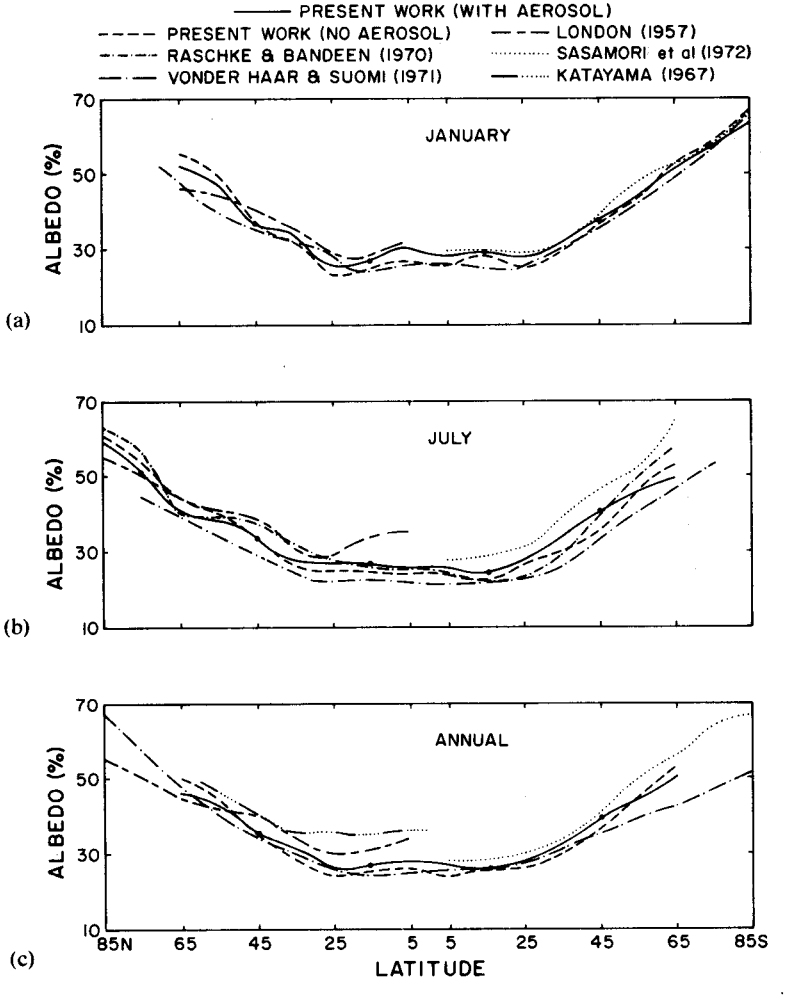

FIG. 12. Zonally averaged planetary albedos: (a) January, (b) July, (c) annual. The dots denote the latitude at which the atmospheric profiles were employed.

although the feature is longer and more pronounced in the present work. Values of surface cooling are in good agreement. The region of heating found at the tropical tropopause is much more distinct in the present work, and the strong cooling of the atmosphere near 30 km in these calculations is much more apparent and stronger than in Dopplick's work.

This comparison is typical of the comparisons for July and January, and for the individual elements of solar heating and longwave cooling. Generally, there is good agreement in the broad-scale features. The differences are quite small in many cases and occur mainly in the smaller features. Such differences as exist are accounted for by differences in the distributions of atmospheric parameters used in the two models, particularly clouds and aerosols, and to a certain extent in the method of calculation used. Dopplick used satellite-derived distributions of cloudiness, but had them classified only as low, middle, or high. He makes no mention of aerosols, so it must be concluded that he did not consider their effect on the heat budget.

5. Effects of Increased Cirrus Cloudiness

The climate of the Earth can be modified to some extent by changes in three basic parameters involved in the radiation balance: changes in the Earth's surface albedo, changes in the chemical and particulate constitution of the atmosphere, and changes in the albedo of the atmosphere (Singer, 1975). A number of mechanisms, both natural and man-induced, are at work presently, causing alterations in these three quantities. The effect of differing surface albedos has been demonstrated in a previous paper (Liou *et al.*, 1978) where the changes in atmospheric heating rates for different surface albedos were computed. The only change in the composition of the atmosphere which has been considered here is the addition of a light background aerosol to a clean atmosphere. These effects were demonstrated in the previous section. The fundamental motivation behind the present work, however, has been to test the response of the atmospheric global heat and radiation budget to an increase in the global albedo and other effects produced by an increase in cirrus cloudiness. Since clouds regularly cover about 50% of the Earth's surface, and since clouds are very good reflectors of solar radiation and good absorbers and emitters of thermal radiation, potential impact of such an increase in cloudiness may be quite large.

Cirrus clouds were chosen for this study because they are found in all latitudes at all seasons, and because their variability on the climatic time scale may be easier to detect than other clouds. Cirrus clouds are rela-

tively stable and long-lived, residing as they do in the upper troposphere and lower stratosphere where they are mostly associated with the large-scale features of the circulation. Other cloud types, lower in the troposphere, are more generally associated with smaller scale circulation features. Thus the cirrus cloud climatology should be fairly well determined, and significant departures from the mean should be easier to detect than for other cloud types.

As described in the Introduction, there is evidence that cirrus cloudiness may well be increasing over North America, the North Atlantic, and Europe. Machta and Carpenter (1971) report secular increases in cirrus clouds over North America during the 22-year period from 1948 to 1970, with most of the increase reported occurring between 1962 and 1966. One suggested reason for the cirrus increase is the steady increase in jet aircraft traffic over the northern hemisphere of the Earth, with these aircraft flying mostly in the upper troposphere and lower stratosphere.

It is well known that jet aircraft deposit large quantities of water in the upper troposphere and stratosphere, mostly in the form of water vapor. One estimate (Study of Man's Impact on Climate, 1971) is that jet aircraft may deposit 2.5×10^{14} gm/yr of H_2O in the vicinity of the tropopause. With residence times for water vapor in the upper troposphere of about 30 days and in the lower stratosphere of 120 days (Landsberg, 1975), the net annual increase in water vapor mixing ratio in the upper troposphere will be about 10^{-4} gm/kg of air and four times that value in the stratosphere. While this additional water vapor content is about two orders of magnitude less than the naturally occurring water vapor in these regions, and thus probably will not be enough to alter the radiative properties of the upper atmosphere, the problem arises because much of the water is emitted in the form of condensation trails. Bryson and Wendland (1975) estimate that the condensation trails may cover as much as 5–10% of the sky in the North America–Atlantic–Europe area, or about 0.8% of the sky globally. Since commercial aircraft flight is estimated to increase by a factor of as much as 3 to 6 in the years 1985 to 1990 (Study of Man's Impact on Climate, 1971), the possibility thus exists for significant increases in cloudiness during the decades to come.

The approach to increasing cloudiness in this study was to assume three models of increasing cirrus amounts. The first model, CIRRUS I, assumes a 5% increase in cirrus cloudiness, at the expense of clear atmosphere, in the latitude bands from 30 to 60° north latitude. The CIRRUS II model assumes an increase of 10% in the same latitude belt, which corresponds generally to the latitudes where cirrus increases have been detected by Machta and Carpenter. Finally, the extreme case,

CIRRUS III, assumes a 20% net increase from 20 to 70° north. These three hypothetical cases could correspond, generally, to possible changes in cirrus cloudiness over the next few years, second, to a more extreme case over the next decade, and finally, CIRRUS III may represent a more serious increase, perhaps augmented by some feedback mechanism.

The basic changes to the heat and radiation budgets expected to result from the increased cirrus cloudiness were increased planetary albedo; reduced solar heating below the cloud and increased cooling above; decreased upwelling longwave flux at the top of the atmosphere, since cirrus clouds are cooler than the ground and are not considered to radiate as blackbodies; and increased downwelling thermal flux at the surface of the Earth, since cirrus clouds are more nearly blackbody radiators than the clear atmosphere. All of these parameters can be deduced from physical reasoning, but the real questions concern the magnitudes of the changes experienced and their net influence upon the radiative budget. Note that since the present model is a steady-state approximation to the atmosphere, no horizontal transports of energy are considered; therefore, any effects due to a change in cirrus cloudiness within a latitude band will be restricted to that band.

The increases in cirrus cloudiness were incorporated into the model through the computer program used to interpolate the solar and terrestrial radiative model results to the appropriate latitudes and seasons. The program was rerun to allow the three cirrus models to be successively implemented while all other parameters were held constant, thereby producing for both the solar and longwave radiation models three new calculations of the radiation field for each month and at each latitude. The results then obtained were compared to the "standard" results presented in the previous section to determine the influence of the three new cloud distributions.

Manabe (1975) estimated that 1% sky coverage of contrails, with assumed cirrus optical properties, would have negligible impact upon the equilibrium temperature of the Earth's surface, but that, if contrails are blackbodies for the terrestrial radiation, an increase of 1% would raise the equilibrium temperature by as much as 0.3°C. In this study, the clouds under consideration were considered to be cirrus and to possess typical cirrus cloud optical properties as described by Liou (1973b, 1974b). They were not, then, considered to be blackbodies for the thermal radiation, but their impact upon the heating of the atmosphere could be detected, nevertheless.

Figures 13 through 15 depict the changes in the heat budget brought about by the three cloud cases. In Fig. 13 for the change in solar heating, it is obvious that the effects of the cirrus clouds are restricted to the level

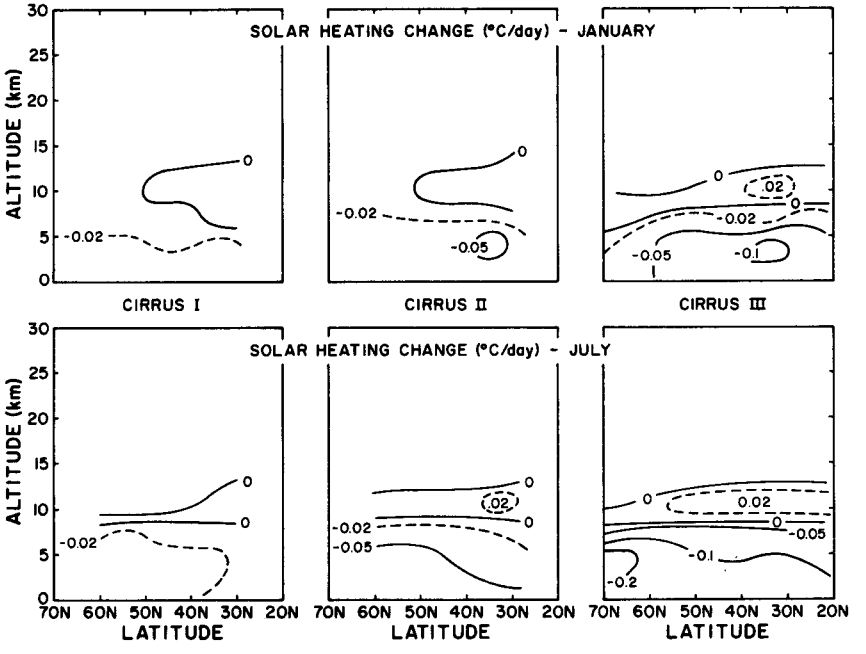

FIG. 13. Changes in the solar heating for January and July conditions due to the increased cirrus cloudiness.

of the cloud and below. Such changes as are indicated above the clouds are very small and are probably due to roundoff in the computation. Within the clouds, or more properly, at the cloud tops, small increases in solar heating are observed, ranging from +0.01°C/day in the CIRRUS I case to +0.04°C/day in the CIRRUS III case in July. Below the cirrus clouds the resulting changes are uniformly in the direction of decreased heating, again ranging in value from −0.01°C/day in the CIRRUS I case to −0.20°C/day in the CIRRUS III calculation.

The reasons for the resulting changes in the solar heating are fairly obvious, since the increased cirrus cloudiness must increase the local albedo (see later) by a small amount, thus reducing the energy available below the cloud for heating the lower atmosphere. The increased heating within the cloud layer is due simply to the fact that solar heating in the cloud is greater than that in the clear atmosphere surrounding the cloud; therefore, increasing the cloud increases the heating relative to the "standard" case. A relatively large increase in albedo produces only very small heating effects in the upper atmosphere. Thus, it is not surprising that the comparatively small changes in albedo produced by the

increasing cirrus clouds produce little or no noticeable effect in the heating above the cloud.

Figure 14 presents comparable results for the longwave cooling budget for January and July. Here, however, it can be seen that the effects of the clouds extend throughout the atmosphere, with drastically different results above and below the cloud layer. Moderate reductions in heating (increased cooling) are observed above the cloud, and rather larger decreases in cooling (increased warming) below the cloud. In the upper troposphere and lower stratosphere, above the clouds, the cooling is intensified by -0.01 to -0.20°C/day while below the cloud the opposite effect; relative warming, is experienced, with magnitudes ranging from $+0.02$ to $+0.36$°C/day. In this case the relative warming in the lower atmosphere is accomplished because the flux divergence in the region is diminished between the blackbody ground surface and the near black cloud base. Above the cloud, cooling is intensified because the flux upward from the warm ground is partially cut off by the increased cloud which has a lower emission temperature. Recall that the cloud is increased at the expense of the clear sky.

The effects upon the net heating of the atmosphere are demonstrated in Fig. 15. Here the increased warming in the longwave band is partially

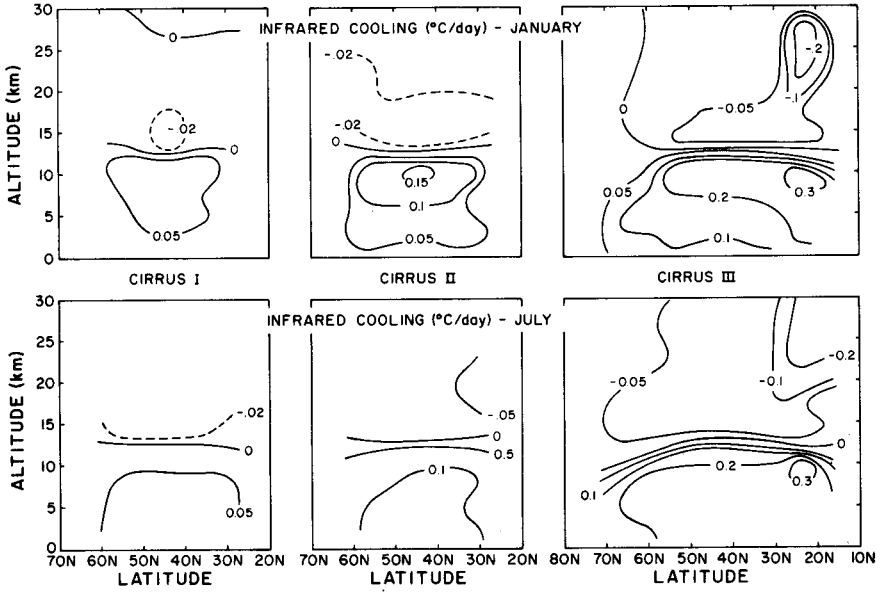

FIG. 14. Changes in the thermal longwave cooling for January and July conditions due to the increased cirrus cloudiness.

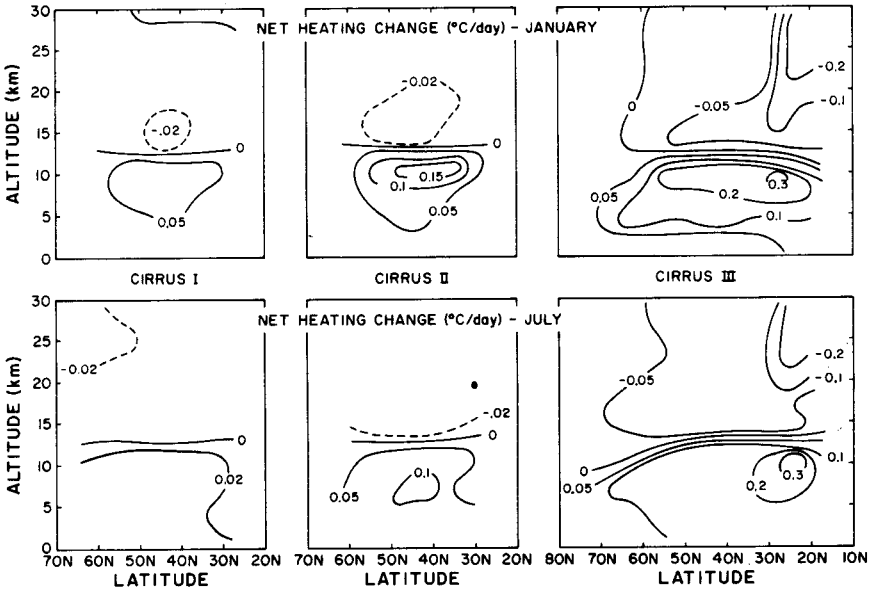

FIG. 15. Net radiative heating changes for January and July conditions due to the cirrus cloudiness.

offset by the cooling in the solar band below the cloud. The small increase of heating by solar radiation within the cloud is supplemented by the longwave warming, and above the cloud the cooling effect is due entirely to the increased cooling by the longwave radiation. The net effects on the heating, averaged over the entire latitude band and height of the atmosphere are very small, only about +0.01°C/day even for the CIRRUS III case. Considering the lower troposphere separately from the upper troposphere and lower stratosphere, however, it is apparent that in the two regions fairly significant effects may be felt. In the lower troposphere the absolute magnitude of the warming effect given by the CIRRUS III model may be as much as 60% of the net annual heating calculated in the "standard" model. In the upper reaches of the troposphere and lower stratosphere, the effect is smaller, but may still be significant, with the absolute value of the cooling increase amounting to as much as 10–15% of the magnitude of the cooling previously calculated. The effects of the CIRRUS I and CIRRUS II models are less, but may still be important, especially in the troposphere.

The heating effects of cirrus clouds on the surface temperature were investigated by Cox (1971) and were determined to be positive (i.e., warming) in the tropical atmosphere and negative (cooling) in the mid-

latitudes. These conclusions were drawn from comparisons of measured cirrus cloud emissivities with a curve of "critical blackness," which was a plot of emissivity against height. The present calculations do not entirely bear out these general conclusions, since the effect of cirrus in every case was to increase the warming in the lower levels of the troposphere below the cloud. There is some similarity, however, since the heating is generally stronger in the tropical atmosphere than at similar levels in the midlatitude and subarctic atmospheres.

To demonstrate the effects of the three cirrus models upon the vertical fluxes of solar and terrestrial radiation, Figs. 16 and 17 show, respectively, the effects upon zonal albedos, absorption of solar radiation by the Earth and atmosphere, upwelling flux at the top of the atmosphere, and downwelling infrared flux at the surface. Only the northern hemisphere data are plotted, since the increased cirrus is restricted to latitude belts in that hemisphere.

As might be expected, the three models show increasing albedos with increases in cirrus cloudiness. This is due to the fact that the reflected

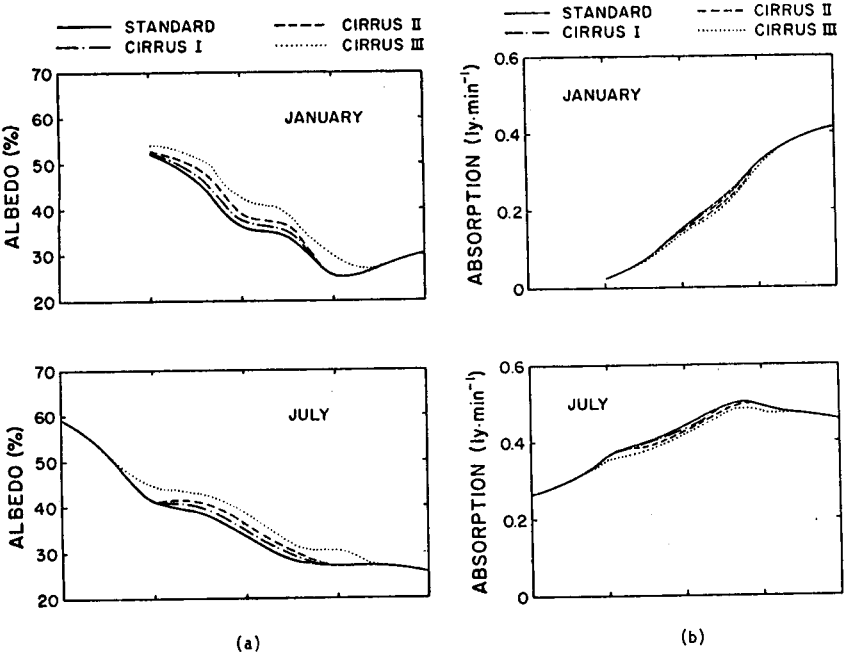

FIG. 16. Zonal albedo (a) and absorption by the Earth–atmosphere system (b) due to the cirrus cloudiness increase for January and July conditions.

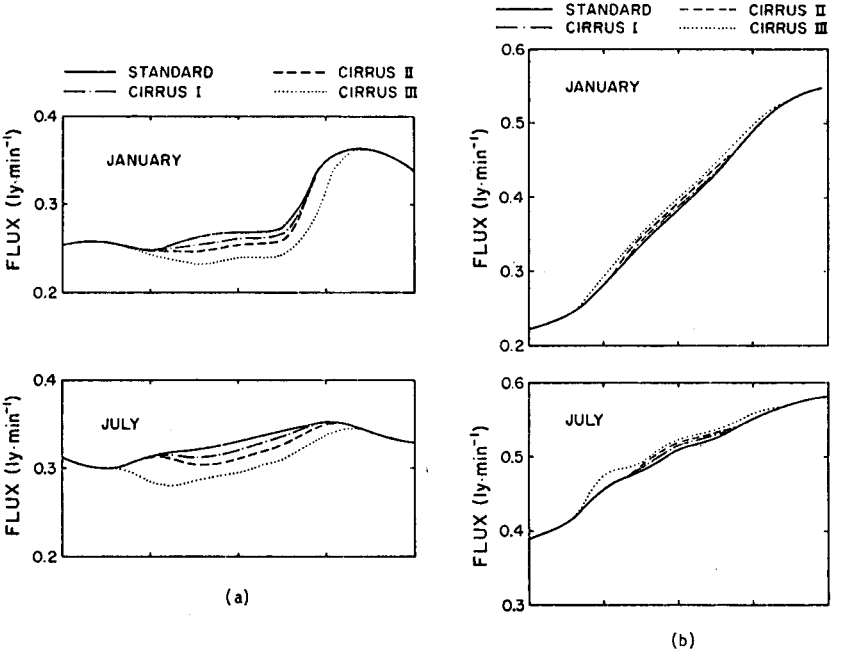

FIG. 17. Upwelling flux at the top of the atmosphere (a) and downwelling flux at the surface (b) due to various cirrus models.

solar flux at the top of the atmosphere containing cirrus clouds was determined to be 18–25% in midlatitudes, while reflection from a clear atmosphere was found to be only 8–13% (both figures are for an overhead Sun, $\mu_0 = 1.0$). The maximum increase for albedo was 6% for the CIRRUS III model in January at a latitude of 45°N. Generally, the increases from the CIRRUS I model were about 1%, and for the CIRRUS II model about 2%. The average increase associated with the CIRRUS III case was 4%.

The major effect of this increase was a reduction in solar flux reaching the lower atmosphere where most of the absorption by gases, clouds, and aerosols takes place. The consequences of this reduced flux are presented in Fig. 16, where the total absorption of solar flux by the atmosphere and Earth is seen to diminish with increasing cloudiness. The decrease was usually less than 1.5% for the CIRRUS I and II cases, while for CIRRUS III the absorption is reduced by as much as 2.6%. The result of this decreased absorption will be felt mainly in the solar heating rates below the cloud, as previously established.

For the longwave portion of the spectrum, the results correspond to those expected previously, where the upwelling flux at the atmospheric top was reduced and the downwelling flux at the ground increased. The alteration in the upwelling flux was large in absolute value than the corresponding change in the downwelling flux. Reductions in the upwelling flux averaged about 2.5% for the CIRRUS I case and about 5% and 10%, respectively, for CIRRUS II and III, while the increases in downwelling flux amounted to only about 0.7%, 1.5%, and 2.9% for the three instances of cirrus increase. This difference can be readily explained, since the cirrus blocks the radiation upward from the warm blackbody surface and reemits radiation from its nonblack top at a much colder temperature. In the case of downward flux, the cirrus clouds essentially block only the emission by ozone and CO_2 in the upper atmosphere. Most of the flux reaching the ground is emitted by water vapor below the cloud, therefore the contribution by the cloud is small.

The combination of changes to these individual elements resulted in alterations to the net radiation budgets for the atmospheric top, the ground, and the net radiation loss for the atmosphere as a whole, as shown in Fig. 18. The net budget at the top of the atmosphere was affected by changes to both the upwelling terrestrial flux and the absorbed solar radiation. Since the fractional decrease in the upward radiation was greater than the decrease in absorption of solar energy, the overall effect was a net increase in the value for the budget at the top of the atmosphere. In other words, the losses in the polar regions were smaller and the gains in the tropics and midlatitudes larger.

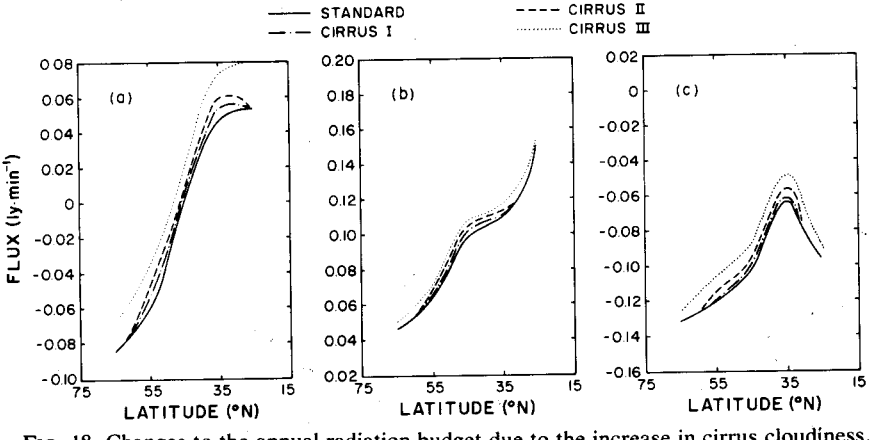

FIG. 18. Changes to the annual radiation budget due to the increase in cirrus cloudiness. (a) Budget for the top of the atmosphere, (b) budget for the surface, (c) net radiation loss for the atmosphere.

At the surface the insolation was reduced by the increased reflection due to the clouds, even though absorption decreased, since the percent change in albedo was larger than the fractional change in absorption. In effect, the energy transmitted to the surface for absorption was lessened. The transmission loss amounted to about 0.7% in CIRRUS I case and to as much as 3% in the CIRRUS III case. In all cases the increase in downwelling flux was slightly larger than the change in surface absorption of solar flux. This lead to a smaller value for the net upward flux at the surface, and consequently, a very small decrease in the surface radiation budget. This implies a small gain in energy for the surface, depending in some measure on the surface albedo, and consequent surface warming.

The net radiation loss by the atmosphere was reduced slightly by the combination of changes resulting from the increased cirrus cloudiness. This loss was a function of the radiation absorbed by the atmosphere, which was reduced by the cloud increase; the upward flux at the top of the atmosphere, which was reduced significantly; and the net upward flux at the surface, which was itself a function of the increased downward flux at the surface and the upward flux at the surface, which remained unchanged. The dominant parameter was the upwelling flux at the top of the atmosphere, which was reduced enough to overcome the decrease in solar absorption, thus leading to a reduction in net radiation loss. These computed changes to the various radiation budget parameters lead to the conclusion that increased cirrus cloudiness may produce some changes in the climatological distributions of heating and energy.

The net effect upon the global radiation balance of an increase in cloudiness is thus the result of two competing fundamental factors. The first factor is the increase in global albedo which causes a decrease in solar energy available to the lower atmosphere. The second factor is a decrease in the loss of infrared radiation to space. The effects of these two factors upon atmospheric heating may be seen in Figs. 13 and 14 where the decreased absorption of solar energy leads to reduced heating in the lower troposphere, while the decreased loss of infrared radiation serves to warm the lower troposphere and cool the upper troposphere and stratosphere. These effects are offsetting to some degree, since this steady state model is not in balance. Over the long term, however, there must be a balance between the absorption of the solar energy and the loss of terrestrial radiation to space. This balance is manifested by the equilibrium blackbody temperature of the Earth–atmosphere system. T_e, and the global average temperature near the surface, T_s.

With changes in the planetary albedo and the Earth's emission of longwave radiation, resulting from the increased cirrus cloudiness, it is reasonable to assume that changes to T_e and T_s will result, and these

parameters are important components of the climate of the Earth. In order to determine the climatic impact of the cirrus models, the changes in T_s and T_e are computed for the new distributions of cirrus cloudiness.

The equivalent blackbody temperature T_e of the Earth–atmosphere system can be determined from [see, e.g., Yamamoto and Tanaka (1972)]

$$\pi R_e^2 S(1 - A_p) = 4\pi R_e^2 \sigma T_e^4$$

where R_e is the Earth's radius, S the solar constant, A_p the global albedo, and σ the Stefan–Boltzmann constant. With the values of global albedo computed from the cirrus models, the equation may be solved for T_e for each case. These results are tabulated in Table VII.

Budyko (1969) gives an empirical expression for the outgoing longwave radiation, I_b, as a function of near-surface temperature, T_s, and global cloud amount, n.

$$I_b = a + bT_s - (a_1 + b_1 T_s)n$$

where $a = -.319$, $b = 0.00319$, $a_1 = 0.0684$, and $b_1 = 0.00228$. I_b is in units of ly min^{-1} and T_s in degrees C. Using the values of I_b computed as a result of the cirrus cloudiness increase, the expression may be solved for T_s. The results of this computation are also given in Table VII.

From Table VII, it may be seen that the effect of increased planetary albedo and reduced longwave flux to space is a reduction in the equivalent blackbody temperature of the Earth–atmosphere system and a reduction in the temperature near the surface of the Earth. This is due to the fact that the increase in albedo is the dominant parameter in determining the net effect. This may not always be so, especially in the case of very thin cirrus, or over areas of very high surface albedo, where the expansion of cirrus coverage may actually lead to a reduction in the planetary albedo, since cirrus clouds reflect solar radiation less strongly than do ice- and snow-covered surfaces.

The temperature reduction is generally quite small in the cases of the CIRRUS I and CIRRUS II models, but becomes significant with the CIRRUS III model, especially for T_s, which is reduced by almost −4°C.

TABLE VII. EFFECTS OF INCREASED PLANETARY ALBEDO AND DECREASED LONGWAVE FLUX ON T_s AND T_e

	Standard	CIRRUS I	CIRRUS II	CIRRUS III
A_p	0.335	0.337	0.339	0.350
T_e (K)	250.7	250.5	250.3	249.2
I_b (ly min^{-1})	0.323	0.322	0.321	0.315
T_s (K)	291.6	290.95	290.65	287.73

The strong decrease in T_s accompanied by only a moderate decrease (-1.5°C) in T_e implies that the atmosphere may be relatively warmed, while the surface is cooled; and indeed, this has been observed above, with a small net warming of the atmosphere occurring in the region affected by the CIRRUS III model.

The area of the globe affected by the CIRRUS III model amounts to about 30% of the Earth's surface, and, while the CIRRUS III model is an extreme case, the implications of an increase in cirrus cloudiness over only a fraction of the globe are serious indeed. Such a large decrease in T_s might, if uncompensated by some negative feedback mechanism, initiate a return to ice age conditions.

Many of the effects of such an increase in cirrus cloudiness must be pure speculation, based as they are upon a steady-state model with many assumptions. Schneider (1972) has computed that while an increase in low and middle level cloudiness would produce cooling on the order of that calculated here, the effect of an increase in globally averaged effective cloud top height would be just the opposite, leading to an increase in surface temperature. Many such coupled mechanisms are at work in the atmosphere, greatly complicating the task of evaluating the results outlined here. The computed changes to the radiation budget parameters lead to the conclusion, however, that increased cirrus cloudiness could produce some changes in the distribution of heating and energy transport in the atmosphere. The ultimate climatological effect of such changes must await evaluation by detailed climate models.

6. Concluding Remarks

In this work the attempt has been made to model the radiation budget of the atmosphere in a more comprehensive manner than previously accomplished and, in addition, to investigate the impact upon that budget of increasing cirrus cloudiness. It is felt that both of these aims have been successfully accomplished.

The radiation budget model has provided, within the limitations of the available data, a useful extension of the work of London, Sasamori, and others. This was accomplished by a more detailed analysis of the effects of aerosol and clouds, particularly their scattering properties. Also, the use of a full radiative transfer model has avoided the employment of parameterizations and empirical formulas which, useful as they are, do not provide the accuracy and flexibility of the present model in describing and quantifying the complex radiation field of the atmosphere.

The radiation model presently employed has allowed a very full ex-

amination of the complex of interactive processes which are going on simultaneously in the atmosphere to produce the radiation budget and atmospheric heating. One process which has been inadequately modeled in the past studies of the radiative balance is scattering. The radiative transfer model used in this work makes use of explicit solutions for Rayleigh and Mie scattering, thus allowing detailed analysis of the contributions of scattering to the atmospheric radiation field with a minimum of simplifying assumptions.

Clouds are the most important atmospheric elements involved in moderating and altering the radiation field, and their effects have been carefully reproduced insofar as possible, although the cloud climatology used was based upon data primarily from the 1940s and before. Cirrus clouds, for reasons described previously, were chosen for particular examination in this work. The variation of cirrus cloudiness was chosen as an independent variable in the computations and the effects of increasing cirrus cloudiness in some near-realistic manner were studied in detail. There are, of course, a number of interactions, particularly interactions of the radiation field with the dynamics of the atmosphere, which have received no attention in this study. The intent of the work, however, was to examine a steady-state model of the radiation field and to test this field by admitting changes in only a single variable.

The effects of cirrus clouds upon the radiation field and heat budget have been demonstrated here, but the climatic impact of such changes has not been modeled. This work has calculated the changes in radiation quantities that would result from the cirrus cloud models employed, but the measure of the influence of these changes upon the climatic distributions of energy and weather has yet to be determined. Such an examination is beyond the scope of the present work, and these long-term influences can best be evaluated by the use of a comprehensive climate model.

ACKNOWLEDGMENTS

This research was supported in part by the Atmospheric Research Section of the National Science Foundation under Grant ATM76-17352. Much of the computational work was performed at the Computing Facility of the National Center for Atmospheric Research.

REFERENCES

Baur, F., and Phillips, H. (1934). Der Wärmehaushalt der Lufthülle der Nordhalbkugel im Januar und Juli und zur Zeit der Aquinoktien und solstien. *Gerlands Beitr. Geophys.* **41**, 160-207.

Bryson, R. A., and Wendland, W. M. (1975). Climatic Effects of Atmospheric Pollution. *In* "The Changing Global Environment" (S. F. Singer, ed.), pp. 139–148. Reidel, Boston, Massachusetts.

Budyko, M. I. (1969). The effect of solar radiation variations on the climate of the earth. *Tellus* **21**, 611–619.

Chandrasekhar, S. (1950). "Radiative Transfer." Dover, New York.

Cox, S. K. (1971). Cirrus Clouds and the climate. *J. Atmos. Sci.* **28**, 1513–1515.

Davis, P. A. (1963). An analysis of the atmospheric heat budget. *J. Atmos. Sci.* **20**, 5–22.

Dopplick, T. G. (1972). Radiative heating of the global atmosphere. *J. Atmos. Sci.* **29**, 1278–1294.

Elsasser, W. M. (1938). On some properties of the water vapor spectrum and their relations to atmospheric radiation. *Mon. Weather Rev.* **65**, 323–326.

Elsasser, W. M. (1942). Heat transfer by infrared radiation in the atmosphere. *Harvard Meteorological Studies* No. 6, Blue Hill Meteorological Observatory, 105 pp.

Elterman, L. (1968). UV, visible, and IR attenuation for altitudes to 50 km. AFCRL-68-0153, 49 pp.

Goldman, A., and Kyle, T. G. (1968). A comparison between statistical model and line by line calculation with application to the 9.6 μm ozone and the 2.7 μm water vapor bands. *Appl. Opt.* **7**, 1167–1177.

Goody, R. M. (1964). "Atmospheric Radiation." Oxford. Univ. Press (Clarendon), London and New York.

Hale, G. M., and Querry, M. R. (1973). Optical constants of water in the 200 nm to 200 μm wavelength region. *Appl. Opt.* **12**, 555–563.

Houghton, H. G. (1954). On the annual heat balance of the northern hemisphere. *J. Meteorol.* **11**, 1–9.

Howard, J. N., Burch, D. L., and Williams, D. (1956). Near infrared transmission through synthetic atmospheres. *Geophys. Res. Papers*, No. 40, Air Force Cambridge Research Labs., Bedford, Massachusetts.

Hunt, G. E. (1977). Studies of the sensitivity of the components of the earth's radiation balance to changes in cloud properties using a zonally averaged model. *J. Quant. Spectrosc. Radiat. Transfer* **18**, 295–307.

Katayama, A. (1966). On the radiation budget of the troposphere over the northern hemisphere: I. Introduction. *J. Meteorol. Soc. Jpn.* **44**, 381–401.

Katayama, A. (1967a). On the radiation budget of the troposphere over the northern hemisphere: II. Hemispheric distributions. *J. Meteorol. Soc. Jpn.* **45**, 1–25.

Katayama, A. (1967b). On the radiation budget of the troposphere over the northern hemisphere: III. Zonal cross-sections and energy consideration. *J. Meteorol. Soc. Jpn.* **45**, 26–38.

Landsberg, H. E. (1975). Man-made climatic changes. *In* "The Changing Global Environment" (S. F. Singer, ed.), pp. 197–234. Reidel, Boston, Massachusetts.

Liou, K. N. (1972). Light scattering by ice clouds in the visible and infrared: A theoretical study. *J. Atmos. Sci.* **29**, 524–536.

Liou, K. N. (1973a). A numerical experiment on Chandrasekhar's discrete ordinate method for radiative transfer: Applications to cloudy and hazy atmospheres. *J. Atmos. Sci.* **30**, 1303–1326.

Liou, K. N. (1973b). Transfer of solar irradiance through cirrus cloud layers. *J. Geophys. Res.* **78**, 1409–1419.

Liou, K. N. (1974a). Analytic two-stream and four-stream solutions for radiative transfer. *J. Atmos. Sci.* **31**, 1473–1475.

Liou, K. N. (1974b). On the radiative properties of cirrus in the window region and their influence on remote sensing of the atmosphere. *J. Atmos. Sci.* **31**, 522–532.

Liou, K. N. (1976). On the absorption, reflection, and transmission of solar radiation in cloudy atmospheres. *J. Atmos. Sci.* **33**, 798–805.

Liou, K. N., and Sasamori, T. (1975). On the transfer of solar radiation in aerosol atmospheres. *J. Atmos. Sci.* **32**, 2166–2177.

Liou, K. N., Freeman, K. P., and Sasamori, T. (1978). Cloud and aerosol effect on the solar heating rate of the atmosphere. *Tellus* **30**, 62–70.

London, J. (1957). A study of the atmospheric heat balance. New York University, Final Report, Contract AF 19(122)-166, 99 pp.

Machta, L., and Carpenter, T. (1971). Trends in high cloudiness at Denver and Salt Lake City. *In* "Man's Impact on Climate" (W. H. Matthews, W. W. Kellogg, and G. D. Robinson, eds.), pp. 410–415. MIT Press, Cambridge, Massachusetts.

Manabe, S. (1975). Cloudiness and the radiative, convective equilibrium. *In* "The Changing Global Environment" (S. F. Singer, ed.), pp. 175–176, Reidel, Boston, Massachusetts.

McClatchey, R. A., Fenn, R. W., Selby, J. E., Voltz, F. E., and Garing, J. S. (1971). Optical Properties of the atmosphere (3rd ed.). AFCRL-72-0497.

Möller, F. (1943). "Das Strahlungsdiagramm." Reichsamt für Wetterdienst, Berlin.

Raschke, E., and Bandeen, W. R. (1970). The radiation balance of the planet earth from radiation measurements of the satellite Nimbus II. *J. Appl. Meteorol.* **9**, 215–238.

Roberts, R. E., Selby, J. A., and Biblerman, L. M. (1976). Infrared continuum absorption by atmospheric water vapor in the 8–12μm window. *Appl. Opt.* **15**, 2085–2090.

Rodgers, C. D. (1967). The radiative heat budget of the troposphere and lower stratosphere. MIT Planetary Circ. Proj., Rep. No. A2, 99 pp.

Rodgers, C. D., and Walshaw, C. D. (1966). The computation of infrared cooling in planetary atmospheres. *Q. J. R. Meteorol. Soc.* **92**, 67–92.

Roewe, D., and Liou, K. N. (1978). Influence of cirrus clouds on the infrared cooling rate in the troposphere and lower stratosphere. *J. Appl. Meteorol.* **17**, 92–105.

Sasamori, T., London, J., and Hoyt, D. V. (1972). Radiation budget of the southern hemisphere. *Meteorol. Monogr.* **13**, (35), Ch. 2.

Schaaf, J. W., and Williams, D. (1973). Optical constants of ice in the infrared. *J. Opt. Soc. Am.* **63**, 728–729.

Schnaidt, F. (1939). Uber die Absorption von Wasserdampf und Kahlensaüre mit besonderer Berücksichtigung der Druck-und Temperatur-Abhängigkeit. *Beitr. Geophys.* **54**, 203–234.

Schneider, S. H. (1972). Cloudiness as a global feedback mechanism: The effects on the radiation balance and surface temperature of variations in cloudiness. *J. Atmos. Sci.* **29**, 1413–1422.

Schneider, S. H., and Dickinson, R. E. (1974). Climate modeling. *Rev. Geophys. Space Phys.* **12**, 447–493.

Shettle, E. P., and Fenn, R. W. (1975). Models of the atmospheric aerosols and their optical properties. *Proc. AGARD Tech. Meet. Opt. Propagation Atmos., 22nd, Lyngby, Denmark, 1975* **183**, 2-1-2-16.

Simpson, G. C. (1928). Some studies in terrestrial radiation. *Mem. R. Meteorol. Soc.* **2**, 70–95.

Singer, S. F. (1975). "The Changing Global Environment." Reidel, Boston, Massachusetts.

Study of Man's Impact on Climate (1971). "Inadvertent Climate Modification." MIT Press, Cambridge, Massachusetts.

Telegadas, K., and London, J. (1954). A physical model of the northern hemisphere

troposphere for winter and summer. New York University, Sci. Rep. No. 1, Contract AF 19(122)-165, 55 pp.

Thekaekara, M. P. (1974). Extraterrestrial solar spectrum, 3000–6100 A at 1-A intervals. *Appl. Opt.* **13**, 518–522.

Thekaekara, M. P. (1976). Solar irradiance: Total and spectral and its possible variations. *Appl. Opt.* **15**, 915–920.

van Loon, H. (1972). Cloudiness and precipitation. *Meteorol. Monogr.* **13**, (35), Ch. 6.

Vigroux, E. (1953). Contribution a l'etude experimentale de l'absorption de l'ozone. *Ann. Phys. (Paris)* **8**, 709.

Vonder Haar, T. H. (1968). Variation of the earth's radiation budget. *Meteorological Satellite Instrumentation and Data Processing*. Final Report, Contract NASA-65, 1958–1968. Univ. of Wisconsin, 179 pp.

Vonder Haar, T. H., and Suomi, V. E. (1971). Measurements of the earth's radiation budget from satellites during a five year period. Part I: Extended time and space means. *J. Atmos. Sci.* **28**, 305–314.

Yamamoto, G. (1952). On a radiation chart. *Sci. Rep. Tohoku Univ. Ser. 5 Geophys.* **4**, 9–23.

Yamamoto, G. (1962). Direct absorption of solar radiation by atmospheric water vapor, carbon dioxide, and molecular oxygen, *J. Atmos. Sci.* **19**, 182–188.

Yamamoto, G., and Tanaka, M. (1972). Increase of global albedo due to air pollution, *J. Atmos. Sci.* **29**, 1405–1412.